4-7-2005

Geochemistry of Serpentinized Peridotites from the Mariana Forearc Conical Seamount, ODP Leg 125: Implications for the Elemental Recycling at Subduction Zones

Ivan P. Savov
University of South Florida, savovi@si.edu

Jeffrey G. Ryan
University of South Florida, ryan@usf.edu

Massimo D'Antonio
University of Naples Federico II

Katherine Kelley
Boston University

Patrick Mattie
University of South Florida

Geochemistry Geophysics Geosystems G3
AN ELECTRONIC JOURNAL OF THE EARTH SCIENCES
Published by AGU and the Geochemical Society

Article
Volume 6, Number 4
7 April 2005
Q04J15, doi:10.1029/2004GC000777
ISSN: 1525-2027

Geochemistry of serpentinized peridotites from the Mariana Forearc Conical Seamount, ODP Leg 125: Implications for the elemental recycling at subduction zones

Ivan P. Savov
Geology Department, University of South Florida, 4202 East Fowler Avenue, SCA 528, Tampa, Florida, USA

Now at Department of Mineral Sciences, National Museum of Natural History, Smithsonian Institution, Washington, DC, USA (savovi@si.edu)

Jeffrey G. Ryan
Geology Department, University of South Florida, 4202 East Fowler Avenue, SCA 528, Tampa, Florida, USA

Now at Division of Undergraduate Education, National Science Foundation, Arlington, Virginia, USA

Massimo D'Antonio
Dipartimento di Scienze della Terra, University Federico II of Napoli, Napoli, Italy

Osservatorio Vesuviano, INGV, Napoli, Italy

Katherine Kelley
Department of Earth Sciences, Boston University, Boston, Massachusetts, USA

Now at Department of Terrestrial Magnetism, Carnegie Institution, Washington, DC, USA

Patrick Mattie
Geology Department, University of South Florida, 4202 East Fowler Avenue, SCA 528, Tampa, Florida, USA

Advanced Environmental Technologies, Inc., Albany, Georgia, USA

[1] Recent examinations of the chemical fluxes through convergent plate margins suggest the existence of significant mass imbalances for many key species: only 20–30% of the to-the-trench inventory of large-ion lithophile elements (LILE) can be accounted for by the magmatic outputs of volcanic arcs. Active serpentinite mud volcanism in the shallow forearc region of the Mariana convergent margin presents a unique opportunity to study a new outflux: the products of shallow-level exchanges between the upper mantle and slab-derived fluids. ODP Leg 125 recovered serpentinized harzburgites and dunites from three sites on the crests and flanks of the active Conical Seamount. These serpentinites have U-shaped rare earth element (REE) patterns, resembling those of boninites. U, Th, and the high field strength elements (HFSE) are highly depleted and vary in concentration by up to 2 orders of magnitude. The low U contents and positive Eu anomalies indicate that fluids from the subducting Pacific slab were probably reducing in nature. On the basis of substantial enrichments of fluid-mobile elements in serpentinized peridotites, we calculated very large slab inventory depletions of B (79%), Cs (32%), Li (18%), As (17%), and Sb (12%). Such highly enriched serpentinized peridotites dragged down to depths of arc magma generation may represent an unexplored reservoir that could help balance the input-output deficit of these elements as observed by Plank and Langmuir (1993, 1998) and others. Surprisingly, many species thought to be mobile in fluids, such as U, Ba, Rb, and to a lesser extent Sr and Pb, are not enriched in the rocks relative to the depleted mantle peridotites, and we estimate that only 1–2% of these elements leave the subducting slabs at depths of 10 to 40 km. Enrichments of these elements in volcanic front and behind-the-front arc lavas point to changes in slab fluid composition at greater depths.

Components: 12,695 words, 12 figures, 7 tables.

Keywords: serpentinite; forearc; mantle; Marianas; subduction; Ocean Drilling Program.

Index Terms: 1031 Geochemistry: Subduction zone processes (3060, 3613, 8170, 8413); 1025 Geochemistry: Composition of the mantle; 3036 Marine Geology and Geophysics: Ocean drilling; 1030 Geochemistry: Geochemical cycles (0330); 8426 Volcanology: Mud volcanism.

Received 15 June 2004; **Revised** 25 October 2004; **Accepted** 21 January 2005; **Published** 7 April 2005.

Savov, I. P., J. G. Ryan, M. D'Antonio, K. Kelley, and P. Mattie (2005), Geochemistry of serpentinized peridotites from the Mariana Forearc Conical Seamount, ODP Leg 125: Implications for the elemental recycling at subduction zones, *Geochem. Geophys. Geosyst.*, *6*, Q04J15, doi:10.1029/2004GC000777.

Theme: Trench to Subarc: Diagenetic and Metamorphic Mass Flux in Subduction Zones
Guest Editors: Gray Bebout, Jonathan Martin, and Tim Elliott

1. Introduction

[2] The Izu-Bonin-Mariana (IBM) arc system presents a unique opportunity to study the operation of the "Subduction Factory" in an intra-oceanic setting. The IBM system differs from other convergent margins in that old, cold lithosphere is subducted, and as there is no geophysical evidence for an accretionary prism [*Horine et al.*, 1990], sediment subduction is probably complete [e.g., *Stern et al.*, 2004]. This arc system is also distinctive in that subduction-related chemical outputs may be sampled at four different "depth steps": at ~20–40 km depths via the forearc serpentine mud volcanoes (seamounts) [*Fryer et al.*, 1992; *Parkinson et al.*, 1992; *Parkinson and Pearce*, 1998]; at ~100–120 km slab depths by the volcanic arc front [*Bloomer et al.*, 1995; *Elliott et al.*, 1997; *Ishikawa and Tera*, 1999; *Straub and Layne*, 2002], via cross-arc seamount chains between 100 and 200 km slab depths [*Hochstaedter et al.*, 2001], and at ~250 km or more in its back-arc spreading systems [*Stolper and Newman*, 1994; *Bloomer et al.*, 1995; *Hochstaedter et al.*, 2001]. For these reasons the IBM system was selected as a focus area for the MARGINS "Subduction Factory" initiative (http://www.margins.wustl.edu/SF/I-B-M/IZUBonin.html). One of the main goals of this initiative is to characterize chemical outputs at each of these four "depth-steps", toward modeling elemental and isotopic mass balances through the IBM system.

[3] Flux imbalances of a number of key geochemical tracers in subduction zones point to the existence of potential outfluxes other than arc and back-arc volcanism. *Plank and Langmuir* [1998] note that for elements like K, Cs and Rb, arc volcanic outputs account for only ~20–30% of the flux input at trenches. For highly soluble trace elements, such as B, Cs, As, Sb and (to a lesser extent) Pb and Rb, data from studies of cross-arc chemical variations show that slab-derived inputs to arc source regions decrease with progressively deeper subduction, reaching mantle-like values in the rearmost centers [*Ryan et al.*, 1996; *Noll et al.*, 1996; *Morris and Ryan*, 2003]. For boron, experimental studies and measurements of fluids from accretionary complexes indicate that fluid releases in proximity to the trenches can account for another 10–20% of the input budget [*You et al.*, 1993, 1995]. Thus less than ~50% of the B subducted in sediments and altered ocean crust (AOC) is accounted for by known arc and trench outputs, and essentially none of this B reaches the deep mantle [*Ryan and Langmuir*, 1993; *Ryan et al.*, 1996; *Ishikawa and Nakamura*, 1994; *Chaussidon and Marty*, 1995]. According to *Bebout and Barton* [1993], the large-scale stable isotope homogenization of Catalina Schist mélange rocks correlates with enormous fluid mobile element (FME) mass transfers and substantial FME depletion at higher metamorphic grades [*Bebout et al.*, 1999]. It is clear that for some species, a substantial, fluid-mediated "return flux" between the trench and the arc is necessary if we are to explain global variations. We report evidence for potentially large material releases from the subducting slab in the IBM system, as recorded in the serpentinized perido-

tites extruded at the Conical Seamount in the Mariana forearc region.

2. Regional Geology

[4] The IBM arc system extends for ~2800 km, from near Mt. Fuji (Japan) to south of Guam (Mariana Islands), where the Mesozoic Pacific Plate is being subducted west-northwestward beneath the Philippine Sea Plate. Subduction in both regions began nearly simultaneously in the Early Eocene, as evidenced by the eruption of boninite and arc-tholeiite lavas on Chichi Jima, the Bonin Islands, and on Guam [*Bloomer et al.*, 1995; *Stern et al.*, 2004]. The Pacific plate descends at a ~20° dip angle to ~60 km depths, while at depths >100 km it sinks abruptly (almost vertically in the Mariana segment, and at ~65° in the Izu-Bonin segment) beneath the Philippine Sea Plate [*Fryer et al.*, 1992]. On the basis of seismic reflection data, *Horine et al.* [1990] concluded that only minor sediment accretion occurred along the Izu-Bonin margin. As with the Izu-Bonin, the nature of dredged samples from the slopes of the Mariana trench (i.e., island arc tholeiites and boninites) suggests little or no current sediment and/or oceanic crustal accretion in the Mariana margin [*Bloomer et al.*, 1995; *Fryer et al.*, 1990, 1992; *Plank and Langmuir*, 1998].

3. Serpentinite Seamounts in the Mariana and Izu-Bonin Forearcs

[5] The basement of the IBM forearc formed after the initiation of arc volcanism and is a consequence of either the trapping of old, most probably Philippine Sea oceanic crust, or intraoceanic rifting caused by island arc volcanism (for discussion, see *DeBari et al.* [1999]). The Mariana forearc preserves a record of extensive vertical movements resulting from seamount collision and fracturing associated with the arc configuration and plate motions over time [*Fryer et al.*, 1985, 1992]. In the IBM system, approximately 50–120 km westward from the Mariana Trench axis, along the trench-slope break (outer-arc high) numerous non-volcanic seamounts occur [*Fryer and Smoot*, 1985; *Fryer et al.*, 1985] (Figure 1). Two types have been described: horst blocks of forearc material, occurring ~0–50 km from the trench; and large serpentinite seamounts, found 50–120 km from the trench, formed by the diapiric protrusion and eruption of serpentine muds (mud volcanoes [*Fryer et al.*, 1992; *Benton*, 1997]). More than twenty of these seamounts have been documented within 120 km of the trench axis in the forearc [*Fryer and Smoot*, 1985; *Fryer et al.*, 1985] (Figure 1). These seamounts are conical in shape, 10–50 km in diameter at their bases, and 500–2000 m high [*Ishii et al.*, 1992].

[6] Conical Seamount lies at 19°31′N Lat., 146°40′W Long., at 3100 m below the sea level. It is 15 km in diameter at the base and 1110 m in height (Figures 2a and 2b), located ~80 km west of the trench axis. Conical Seamount is considered active because of the discovery of recent mud extrusions and the venting of fresh fluids with deep slab origins [*Mottl*, 1992; *Fryer and Mottl*, 1992]. Three holes were drilled in the Conical Seamount during the ODP Leg 125: two on the flanks (Sites 778 and 779) and one at the summit (Site 780) [*Fryer et al.*, 1990] (Figure 2a).

4. Sample Selection and Analytical Methods

[7] A suite of serpentinized peridotite clasts from the Conical seamount was selected for this study. These rocks are usually recovered as dense, cm-sized clasts, surrounded by a fine-grained mud matrix (serpentinite mud). Our intent was to select samples that record conditions of maximum peridotite-slab fluid exchange at depth, so samples were chosen to include vein-rich and heavily serpentinized clasts with high loss on ignition (LOI) values (often >12%). Textural and mineralogical relationships of veined samples were examined in thin sections using standard petrographic techniques. Samples for bulk rock analysis were crushed and powdered using an alumina ball mill (for major elements) and/or an agate mill (for trace elements). Major and some trace element (Cr, Ni, V, Co, Sc, Zn, Cu, Sr, Ba, Mn) abundances were analyzed at the University of South Florida by direct current plasma-atomic emission spectrometry (DCP-AES) following HF-$HClO_4$ acid digestions, or following $LiBO_2$ fluxed-fusion digestions. $LiBO_2$ fluxed-fusion digestion techniques follow those described by *Savov et al.* [2001] in that furnace temperatures were maintained at 1125°C to encourage complete digestion of ultramafic samples. HF-$HClO_4$ methods for major and trace element analysis followed our procedures for Li determinations (see below), save that as a final step, an aliquot of the sample solution was diluted 1:1 with a 2000 ppm Li solution (made with ultrapure Li_2CO_3), to negate matrix effect problems which can occur during DCP-AES analysis. The

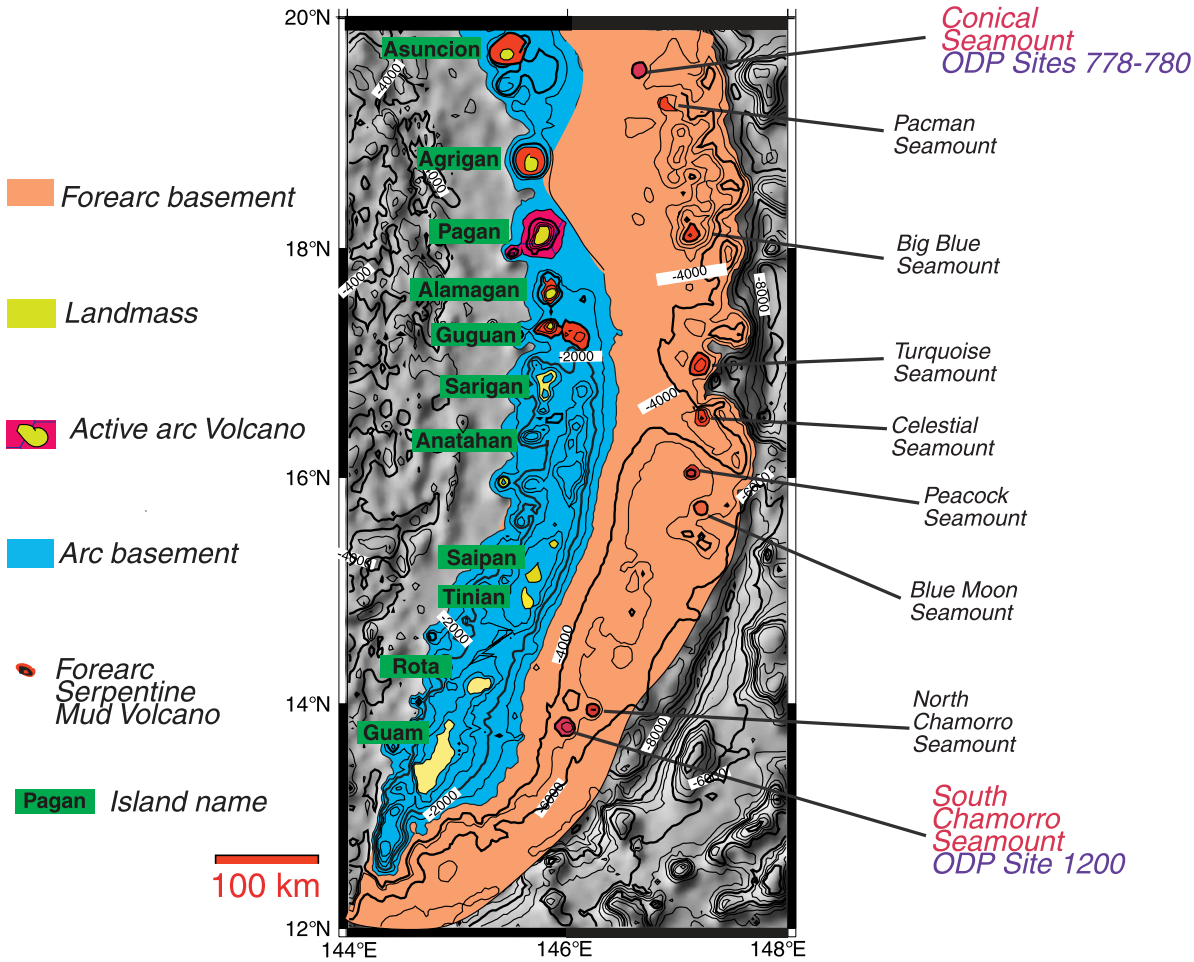

Figure 1. Map of the Mariana arc-basin system showing the location of Conical Seamount (ODP Leg 125), S. Chamorro Seamount (ODP Leg 195), and other serpentinite seamounts in respect to islands of the volcanic front. Modified after *Fryer et al.* [1999].

HF: $HClO_4$ method permitted the measurement of all major elements save SiO_2 (lost as volatile SiF_4 during drydown) and many lithophile trace elements. Commonly, chromite does not dissolve well via HF methods, but little or no chromite was encountered in the extensively serpentinized and hydrated samples we chose for geochemical analysis. Replicate analysis of IWG standard UBN-1, GSJ standard JP-1, and USGS standards DTS-1, BHVO-1 and BIR-1, document precision for major elements between ±1% and ±3%.

[8] Lithium abundances were measured by DCP-AES, following the HF: $HClO_4$ sample digestion procedures of *Ryan and Langmuir* [1987]. All Li measurements were performed by standard additions techniques, using a gravimetric Li standard made from ultra-pure Li_2CO_3. Reproducibility of our Li determinations was ±5% at the 1 ppm Li level. B abundances were measured at USF via DCP-AES following a Na_2CO_3 fluxed fusion method modified from that of *Ryan and Langmuir* [1993] in that as a final step, all solutions were neutralized with ultra-pure HNO_3, and no column preconcentration procedures were used. Since the majority of the measured serpentinites have B abundances >10 ppm, reproducibility of B measurements for this study was ±5%.

[9] A subset of serpentinites was analyzed for rare earth elements (REE), Y, Sr, Rb, Cs, Pb, As, Sb, U, Th, Nb, Ta, Hf, Zr, Sc, V, Ga, Cu and Zn using the VG Elemental PlasmaQuad II ICP-MS facility at the Department of Earth Sciences of Boston University. Samples were digested in 3:1 HNO_3: HF mixtures, following procedures described by *Kelley et al.* [2003]. Gravimetric calibration standards were matrix-matched to sample solutions by adding ~150 ppm Mg from a 1000 ppm Mg standard solution (SPEX, Metuchen, NJ). Concentrations of

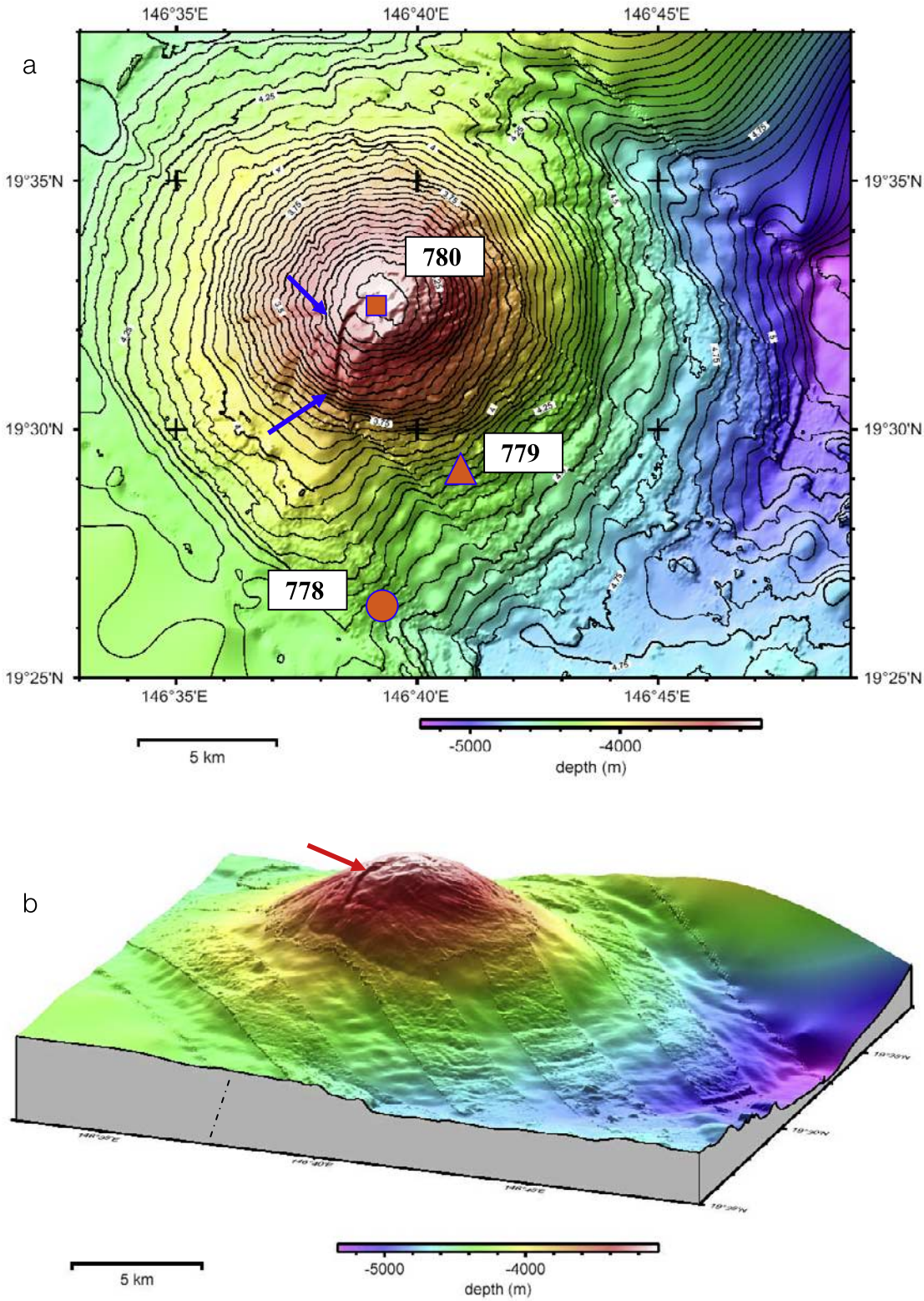

Figure 2. (a) Plane view of the Conical Seamount. Note the traces of possible fault escarpment (marked with arrows). The locations of Holes 778, 779, and 780 are shown as a circle, a triangle, and a square, respectively. (b) Three-dimensional view of the Conical Seamount (ODP Leg 125). Note that in less than 10 km to the west of Conical Seamount the water depth exceeds 5 km.

all these elements were reproducible to ~±2%, based on monitoring by replicates of the certified standards JB-3, BIR-1, AGV-1, JP-1 and DTS-1. Comparisons to standards reveals an accuracy of about ±5% for higher concentration elements, and about ±10% for the lowest concentration elements, such as Zr, Hf, Th, Nb, As, and Sb.

[10] Sr isotope measurements were carried out at Osservatorio Vesuviano (INGV, Naples, Italy). Sr was extracted via conventional ion-exchange chromatographic techniques in an isotope clean laboratory facility. Measurements were made by thermal ionization mass spectrometry (TIMS) techniques on a ThermoFinnigan Triton TI multi-collector mass spectrometer running in static mode. The normalization value for fractionation of $^{87}Sr/^{86}Sr$ was $^{86}Sr/^{88}Sr = 0.1194$. External precision (2 sigma) for Sr isotope ratios from successive replicate measurements of standards was better than 10 ppm for the SRM-987 International Reference Standard for Sr (average $^{87}Sr/^{86}Sr = 0.710249$; N = 29; standard deviation = 6.6×10^{-6}). The total blank for Sr was negligible for the measured samples during the period of measurements.

5. Results and Discussion

5.1. Petrography and Metamorphism

[11] New petrographic observations described here are based on several vein-rich, heavily serpentinized peridotite thin sections. The nomenclature for serpentinization textures used in this study are after *O'Hanley* [1996]. When serpentinization is not advanced, our observations are in overall agreement with the observations of *Parkinson and Pearce* [1998] and the ODP Leg 125 Scientific Party [*Fryer et al.*, 1992]. In hand specimen the serpentinized peridotites range in color from deep blackish-green to light gray. Away from the veins, most have massive fabrics, but some show small-scale foliation and lineation, caused by alignment of bastitic orthopyroxene. Among all of the recovered serpentinized rocks from Leg 125, the predominant protoliths are harzburgites and dunites. The less serpentinized samples examined here and by *Parkinson and Pearce* [1998] preserve evidence of their peridotite protoliths. Rock textures are protogranular and less commonly porphyroclastic. Relict olivines occur as small crystals (mm size) with curved contours and traces of recrystallization. Orthopyroxene occur as small (1–10 mm) and irregularly shaped grains (Figure 3). Orthopyroxene is often altered to serpentine and commonly preserves the "herringbone" texture of clinopyroxene exsolution lamellae. According to *Ishii et al.* [1992], the orthopyroxene is Mg-rich enstatite with low CaO (<0.2–0.6 wt%) and Al_2O_3 (~2 wt%). Clinopyroxenes (typically diopsides) are usually small in size (0.1–1 mm), and occur between or inside orthopyroxene grains. The original spinel phase is chromite (Cr # reaching ~80) [*Parkinson and Pearce*, 1998] and when found it occurs in close association with orthopyroxene (Figure 3).

[12] The examined ultramafic clasts are all 70% to 100% serpentinized. As noted by *Saboda et al.* [1992] and *Zack et al.* [2004], chrysotile and lizardite are common in the Mariana forearc serpentinites, while antigorite is typically absent or very rare. These observations reveal that the alteration of the Leg 125 peridotites records low temperatures (<250 C°), where olivine is altered to mesh-textured lizardite, orthopyroxene to bastitic lizardite, and many of the clasts are cross-cut by complicated sets of serpentine (mostly chrysotile) veins (Figure 3). Sometimes LOI values exceed those characteristic for serpentine minerals of 13–14% [*O'Hanley*, 1996]. However, the samples with elevated LOI's do not show elevated CaO (or lowered MgO contents), indicating the absence of carbonates and the presence of abundant brucite in these samples.

[13] The maximum pressure-temperature metamorphic conditions of the Mariana forearc samples are lower than the lawsonite-albite metamorphic facies from the Catalina Schist [*Bebout*, 1995; *Bebout et al.*, 1999]. The preponderance of low temperature serpentine minerals is consistent with recently proposed models of forearc metamorphic conditions between 20 to 40 km depths of *Hyndman and Peacock* [2003] (i.e., the scarcity of antigorite and the abundance of chrysotile, occurs at depths <35 km and temperatures <250°C). Metamorphic conditions in the Mariana forearc may reflect lower temperatures because the IBM forearc crust is thin, allowing the mantle underneath to cool more efficiently. The presence of Na-rich amphiboles in the mud matrix enclosing the serpentinized peridotites [*Fryer et al.*, 1999; P. Fryer et al., Origins of serpentinite muds from Mariana forearc seamounts, submitted to *Earth and Planetary Science Letters*, 2004] indicates high pressures [see *Gharib et al.*, 2002]. When present, the antigorite and Na-rich amphiboles may indicate that

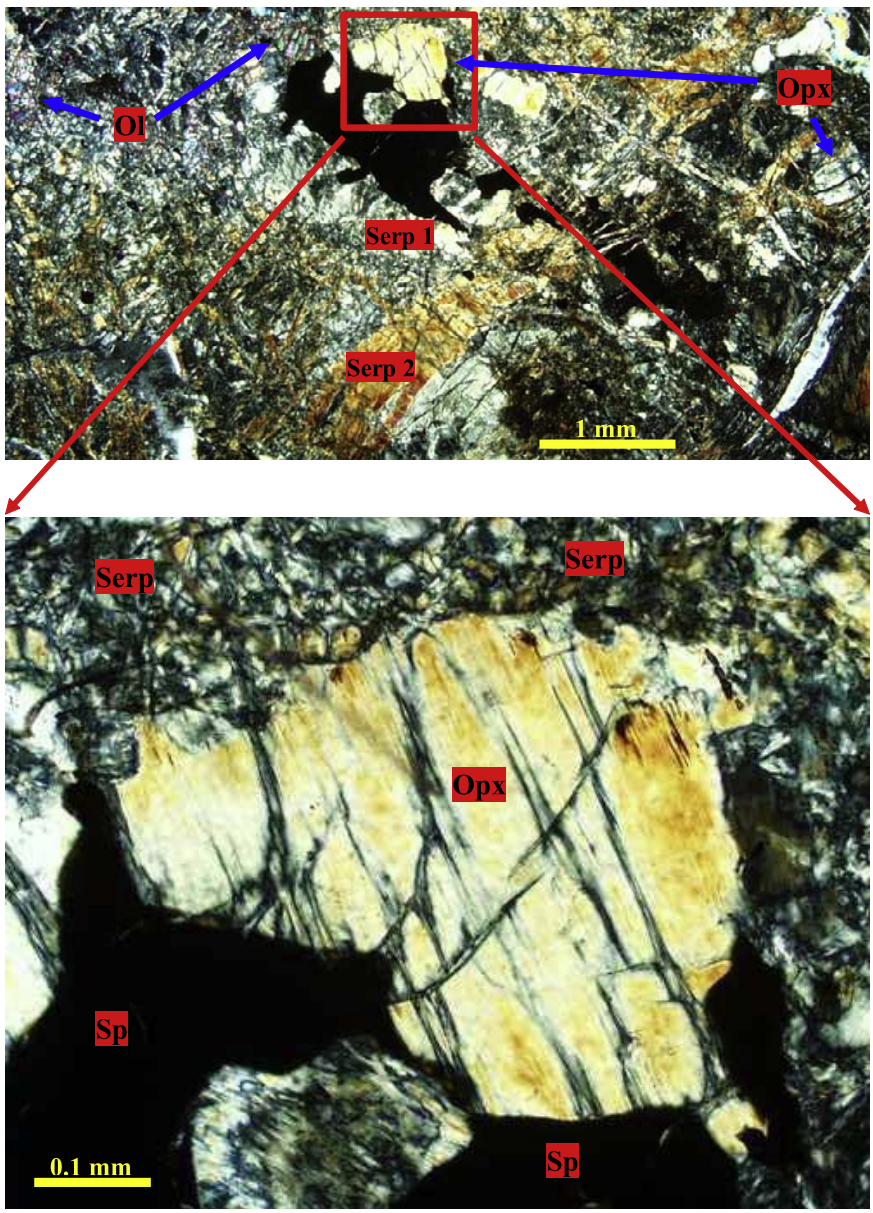

Figure 3. Photomicrographs of serpentinized peridotite sample 779A-26R-2-72-75, showing relics of fresh olivine (Ol), orthopyroxene (Opx) and spinel (Sp), plus several serpentine varieties: massive (Serp 1) and vein-filling (Serp 2). The square on the top photomicrograph marks the area shown on the photomicrograph at the bottom. Cross polarized light.

these particular clasts record slightly deeper conditions, where temperatures and pressures were higher.

5.2. Bulk Rock Geochemistry of the Clasts From Conical Seamount

5.2.1. Major Element Variations

[14] No species in any Leg 125 site, including the fluid-mobile alkaline elements and Sr isotopes, show correlations with LOI values (Figures 4 and 5). Immobile trace element ratios, such as La/Yb, Zr/Yb, Hf/Yb and Nd/Yb, remain relatively unchanged with increasing LOI (Figure 6). All of our samples are extensively serpentinized, with average LOI values approaching 14% in both sites (Figures 4 and 5). Samples from Site 780 differ slightly from those of Site 779A in overall lower average abundances of MgO, Cr, TiO_2 and Sr, and higher Ni, Al_2O_3 and Li (Figure 7, Tables 1 and 2). With the exception of higher average LOI, our major element results are in reasonable agreement

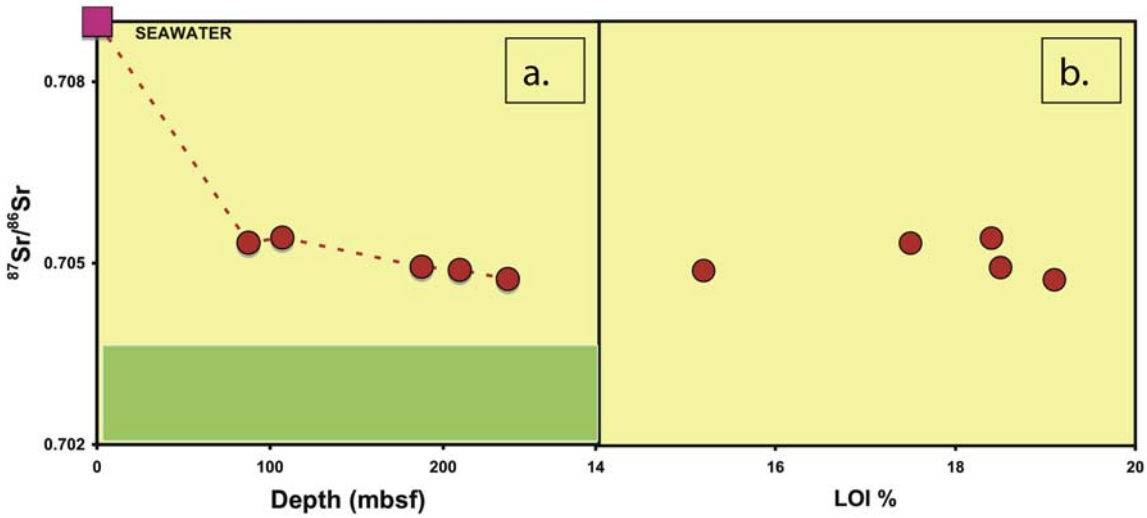

Figure 4. Variation of $^{87}Sr/^{86}Sr$ ratio (a) with increasing core depth and (b) Loss on Ignition (LOI). Values for depleted mantle are from *Salters and Stracke* [2004]. Ambient seawater $^{87}Sr/^{86}Sr$ values are from *Haggerty and Chaudhuri* [1992].

with those of *Parkinson and Pearce* [1998]. Although during serpentinization MgO mobilization is well documented, the magnitude of MgO change is small, so reasonable inferences about mantle protoliths for the serpentinites can be made on the basis of variations among key major elements. Our Leg 125 serpentinites are uniformly low in Al_2O_3, indicating strongly depleted mantle protoliths (Figure 8). As a whole all of the samples are Mg-rich, with high average Ni and Cr contents (2250 and 2525 ppm, respectively). The Mg numbers in our samples range from 91 to 93.

5.2.2. Fluid Mobile Element (FME) and Large Ion Lithophyle Element (LILE) Variations

[15] The B abundances of serpentinized peridotite clasts from Conical Seamount decline from ~60 ppm close to the ocean floor to an average value of ~16 ppm below 60 mbsf (Figure 9a). Boron abundances correlate positively with LOI at Site 780C, but show no such correlation for the other drill sites. Similar downhole declines in B abundance was observed in the Leg 125 serpentinite mud data set of *Benton et al.* [2001] and *Savov* [2004], as well as in the Leg 125 pore water data set of *Mottl* [1992]. As seawater contains ~4.4 ppm boron [*Mottl*, 1992], the averages and the range for B concentrations were calculated for serpentinized peridotites recovered below the core depth intervals affected by seawater. At these core depths, boron concentrations tend to be uniform. A detailed description of the boron systematics at Conical Seamount sites 779 and 780 is given by *Benton et al.* [2001].

[16] Arsenic and cesium contents of the Site 780 samples range from 0.15 ppm to 0.74 ppm and 0.12 ppm and 0.44 ppm, respectively, with average

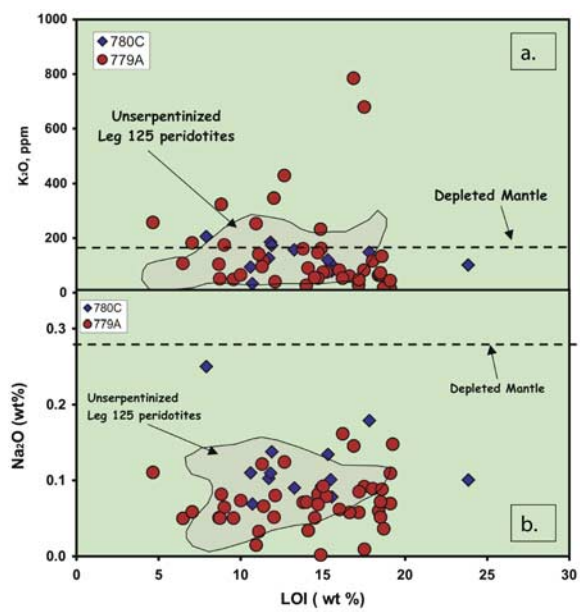

Figure 5. Variation of alkaline elements and element ratios with LOI: (a) K_2O and (b) Na_2O. The depleted mantle values are from *Salters and Stracke* [2004]. Note that the range for unserpentinized peridotites [after *Parkinson et al.*, 1992; *Parkinson and Pearce*, 1998] overlaps quite well with the one for the serpentinized peridotites.

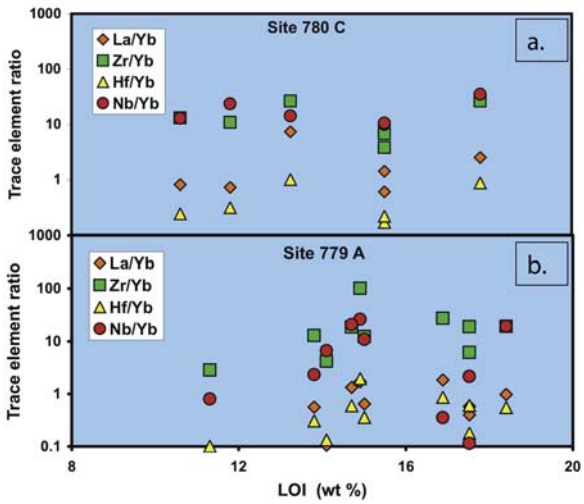

Figure 6. Variation of HFSE/HREE (Yb) ratios with LOI for ODP Sites (a) 780C and (b) 779A. [La/Yb], diamonds; [Zr/Yb], squares; [Hf/Yb], triangles; and [Nb/Yb], circles. Note that the variations of the above elemental ratios are always independent of the LOI values.

Site 780 As = 0.355 ppm and Cs = 0.18 ppm. Serpentinized peridotites from Site 779 have similar Cs abundances (average = 0.16 ppm), but higher average As (~0.73 ppm) (Figures 9b and 9c). The As abundances are very high compared to the 7 ppb As depleted mantle value suggested by *Salters and Stracke* [2004]. Our As contents are an order of magnitude higher than As concentrations we have measured in serpentinized abyssal peridotites samples from ODP Sites 637A, 897D, 920D and 895D (average = 0.05 ppm) and that of San Carlos mantle xenolith (As = 0.065 ppm) (R. P. Price and I. P. Savov, unpublished data). The Leg 125 samples show broad correlations between B/La and As/Ce ($R^2 = 0.87$) and between B/La and Cs/Ce ($R^2 = 0.63$). Antimony contents in Leg 125 serpentinized peridotites (Site 779A: Sb = 0.0359 ppm; Site 780C: Sb = 0.019 ppm) are enriched relative to depleted mantle values (Figure 9d). As with arsenic and cesium, we observe no systematic downhole Sb variations.

[17] Lithium is enriched in our serpentinized peridotites to a slightly lesser degree than As and Cs. The average Li content of our samples is ~4.6 ppm (Site 779A: Li = 3.9 ppm and Site 780C Li = 6.3 ppm [see also *Benton et al.*, 2004]). Our bulk rock Li abundances are similar to those of abyssal serpentinites we have analyzed from other ODP Sites (637A, 897D, 920D and 895D), and are comparable to the abundances reported by *Decitre et al.* [2002]. Conical Seamount Li abundances are clearly elevated relative to those of the inactive Torishima Seamount in the northern Marianas (average Li = 2.4 ppm) and to the depleted mantle (Figure 9e). The lithium enrichments observed in forearc serpentinized peridotites, coupled with extremely low pore water Li contents [*Mottl*, 1992], and the extremely high δ^7Li of such fluids [*Savov et al.*, 2002], provide new constraints on the mechanisms for input, storage, and distribution of moderately fluid-soluble elements in mantle sources [see also *Benton et al.*, 2004]. The behavior of lithium, arsenic and cesium during shallow sub-

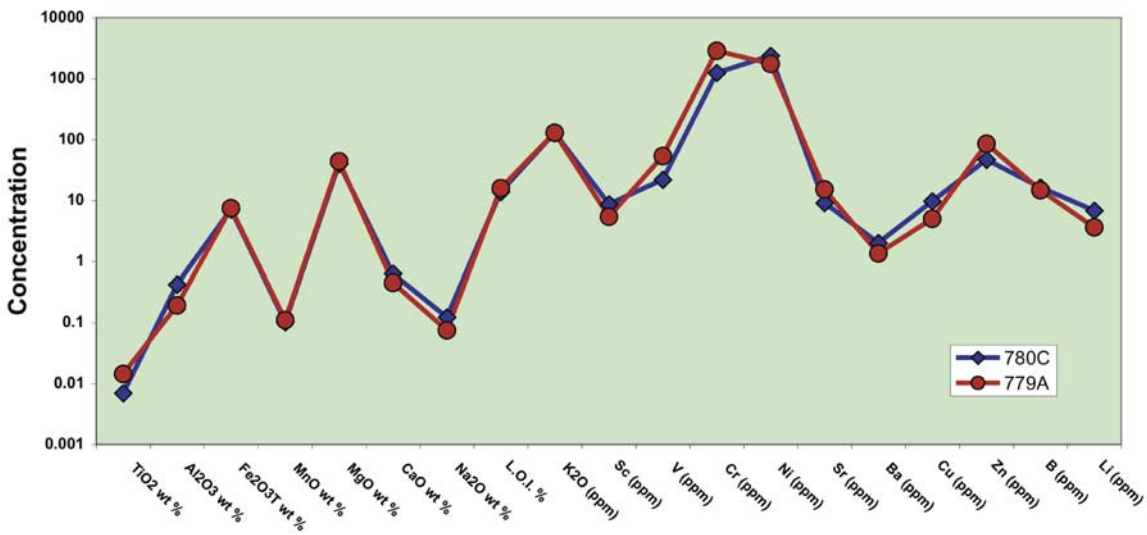

Figure 7. Multielement plot comparing some of the average major and trace element concentrations of serpentinized peridotites recovered from Sites 779A (circles) and 780C (diamonds). All oxides and LOI are in wt%; all others are in ppm.

Table 1a. DCP-AES Major and Some Trace Element Data for Serpentinized Peridotites From Conical Seamount Site 780C[a]

	Core and Section											
	03R-01	06R-01	08R-01	08R-01	09R-01	010R-01	012R-01	013R-01	016R-01	018R-01	018R-01	018R-01
Interval and piece number	(32–33) # 3A	(63–65) # 7a	(39–41) # 5	(100–101) # 10	(51–52) # 6	(15–16) # 2	(16–17) # 2	(43–44) # 7	(52–53) # 7	(16–17) # 2A	(55–57) # 2A	(113–114) # 2B
Depth, mbsf	14.32	43.13	61.89	62.45	71.61	80.9	100.36	106.93	135.52	154.16	154.55	155.13
TiO_2, wt%	0.01	0.006	0.002	0.008	0.011	0.007	0.005	0.007	0.006	0.007	0.002	0.012
Al_2O_3	0.12	0.45	0.06	0.64	0.34	0.53	0.21	0.76	0.63	0.04	0.55	0.78
Fe_2O_3T	5.33	7.06	6.12	7.87	7.49	7.09	6.97	7.65	6.84	8.10	7.38	7.38
MnO	0.08	0.10	0.09	0.11	0.11	0.10	0.10	0.11	0.11	0.11	0.11	0.11
MgO	31.58	40.13	36.47	41.76	44.05	39.58	40.29	41.53	40.07	42.90	39.09	39.79
CaO	0.20	0.69	0.36	0.51	0.68	0.82	0.34	0.98	0.76	0.32	0.85	1.02
Na_2O	0.09	0.10	0.18	0.11	0.10	0.11	0.14	0.25	0.13	0.08	0.07	0.10
K_2O, ppm	157	127	149	95	108	186	174	207	120	79	34	102
L.O.I., %	13.25	11.7	17.82	10.6	15.47	11.8	11.88	7.9	15.3	15.54	10.7	23.85
Sc, ppm	5.7	10.2	4.7	9.5	7.0	9.8	7.4	12.2	10.1	5.4	11.0	12.0
V	11.5	23.7	9.6	26.4	16.7	26.8	13.0	35.6	25.4	8.9	28.7	36.4
Cr	929.1	1066.0	921.9	1855.0	716.6	1439.2	687.5	2477.5	1353.4	368.0	1173.8	2051.9
Ni	1927.7	2396.7	2352.8	2450.3	2427.1	2380.5	2253.3	2495.5	2563.3	2695.1	2492.1	2362.4
Sr	8.5	3.9	22.3	3.7	13.4	8.6	8.9	0.7	25.6	11.2	0.5	1.4
Ba	2.8	1.4	2.0	1.4	1.6	4.7	3.6	0.9	2.8	1.4	0.7	0.9
Cu	8.0	6.4	7.4	4.8	11.1	5.8	6.7	10.9	11.7	11.4	12.1	19.3
Zn	47.1	38.6	55.7	44.4	34.6	43.0	41.2	57.8	60.3	41.7	38.9	54.2
B	21.2	10.89	40.9	10.99	12.12	3.9	11.7	7.1	58	7.22	0.393	12.1
Li	18.9	3.2	1.9	11.8	1.6	4.7	16.2	9.4	4.2	2.3	2.7	4.5

[a] Oxides and LOI in weight percent, all other elements in ppm. See text for analytical precision.

duction resembles that of boron, suggesting that these species may move readily off the slab and into the mantle at very low temperatures.

[18] The solubility of large-ion incompatible trace elements such as K, Sr, Rb and Ba has been suggested on the basis of serpentinite decomposition experiments at high pressure [*Tatsumi and Nakamura*, 1986], and by the abundances of these elements in phengites and amphiboles in the ~2 GPa eclogites from Trescolmen (Central Alps) [*Zack et al.*, 2001]. However, our Conical Seamount samples show abundances of these elements that are similar to, or only modestly elevated relative to mantle values (Figure 6, Figures 9g and 9h). Potassium and rubidium contents modestly higher than seawater in Conical Seamount pore waters point to some mobility of these species in the forearc, but not to their substantial removal from the slab at shallow depths. Both Sr and Ba are markedly depleted in Conical seamount pore waters [*Mottl*, 1992], indicating very limited mobility and restricted transport off the slab.

5.2.3. Uranium-Thorium-Lead Systematics

[19] Compared to the depleted mantle, serpentinized peridotites from Conical Seamount have slightly elevated Pb abundances (Figure 8i), and similar U and Th abundances (Figures 9j and 9k). One sample from Site 780C [(3R-01-(31–33)], has anomalously high Pb (2.5 ppm), Th (0.024 ppm) and U (0.007 ppm). This particular clast is from a very shallow core depth (14.3 mbsf) and may have been contaminated during recovery.

[20] The hydrated peridotites from the Mariana forearc region are highly residual [*Parkinson et al.*, 1992; *Parkinson and Pearce*, 1998] and thus might be expected to have high U/Th ratios. According to *Sun and McDonough* [1989] $D_{Th} < D_U$, which means U/Th will increase with increasing extents of melting. Also, since U shows fluid-mobile behavior in some arc settings [*Turner et al.*, 1997] while Th does not [*Reagan et al.*, 1994], subarc mantle peridotites may also gain uranium from U-enriched slab-derived fluids and/or melts in regions of arc magma generation.

[21] *Plank and Langmuir* [1998] observed an imbalance between the subducting inventory of U and its releases at arcs and back-arcs [see also *Elliott et al.*, 1997; *Noll et al.*, 1996, and references therein]. This imbalance requires that either some U be returned to surface reservoirs before subducting slabs reach the deep mantle, or that U remain on

Table 1b. DCP-AES Major and Some Trace Element Data for Serpentinized Peridotites From Conical Seamount Site 780C[a]

	Core and Section						
	03R-01	08R-01	08R-01	09R-01	010R-01	013R-01	018R-01
Interval and piece number	(32–33) # 3a	(39–41) # 5	(100–101) # 10	(51–52) # 6	(15–16) # 2	(43–44) # 7	(16–17) # 2A
Depth, mbsf	14.32	61.89	62.45	71.61	80.9	106.93	154.16
Li	18.1	1.5	9.8	0.5	3.2	7.6	1.3
Sc	4.18	2.86	7.52	4.83	7.55	9.11	3.71
TiO_2, wt%	0.004	0.003	0.004	0.009	0.004	0.008	0.002
Cr	967.5	371.5	4507.8	2304.5	3158.2	5185.4	1024.1
Co	111.4	124.6	115.7	103.9	111.1	122.3	125.0
Ni	2392.1	2486.8	2256.2	2162.8	2136.4	2129.1	2502.5
Cu	3.7	3.7	1.6	11.4	4.6	5.4	7.2
Zn	34.7	50.7	30.6	25.8	28.1	40.2	36.8
Ga	0.18	0.11	0.51	0.23	0.32	0.58	0.08
As	0.3	0.4	0.7	0.2	0.1	0.4	0.3
Rb	0.82	0.68	0.40	0.56	1.05	0.26	0.31
Sr	7.85	20.53	3.19	11.56	7.25	0.70	10.25
Y	0.14	0.01	0.07	0.08	0.02	0.07	0.01
Zr	0.37	0.08	0.27	0.06	0.13	0.08	0.05
Nb	0.197	0.109	0.271	0.159	0.284	0.402	0.075
Cs	0.26	0.09	0.25	0.14	0.44	0.01	0.07
Ba	2.44	1.71	1.04	1.33	4.46	0.9	0.87
La	0.1022	0.0079	0.0171	0.0097	0.0089	0.0283	0.0102
Ce	0.1271	0.0300	0.0607	0.0529	0.0424	0.0332	0.0532
Pr	0.0251	0.0018	0.0047	0.0029	0.0021	0.0072	0.0030
Nd	0.0890	0.0065	0.0201	0.0084	0.0070	0.0244	0.0096
Sm	0.0205	0.0003	0.0028	0.0002	0.0003	0.0055	0.0004
Eu	0.0027	0.0012	0.0017	0.0007	0.0016	0.0005	0.0007
Gd	0.0221	0.0009	0.0042	0.0031	0.0004	0.0066	0.0006
Tb	0.0042	0.0001	0.0009	0.0009	0.0001	0.0013	0.0001
Dy	0.0248	0.0007	0.0066	0.0082	0.0012	0.0092	0.0008
Ho	0.0052	0.0002	0.0021	0.0024	0.0005	0.0029	0.0003
Er	0.0144	0.0010	0.0096	0.0091	0.0036	0.0119	0.0019
Yb	0.0137	0.0031	0.0210	0.0160	0.0121	0.0243	0.0071
Lu	0.0021	0.0009	0.0047	0.0033	0.0028	0.0052	0.0018
Hf	0.014	0.003	0.005	0.003	0.004	0.004	0.002
Pb	2.493	0.030	0.040	0.011	0.026	0.084	0.009
Th	0.0244	0.0012	0.0019	0.0002	0.0004	0.0035	0.0005
U	0.0072	0.0010	0.0014	0.0002	0.0002	0.0016	0.0003
Sb	0.004	0.005	0.029	0.067		0.006	0.005

[a] Oxides and LOI in weight percent, all other elements in ppm. See text for analytical precision.

the slab and be transported to the deep mantle. Oxidizing slab-derived fluids, in which hydroxylated forms of U^{6+} are much more soluble than Th^{4+} [*Bailey and Ragnarsdottir*, 1994], could potentially produce elevated fluid U/Th. However, the pore fluid results of *Mottl* [1992] document that Leg 125 pore fluids are reducing. On the basis of these pore fluid studies, and the very low U and Th abundances in the serpentinites, we suggest that in the Mariana forearc uranium behaves less like a truly H_2O mobile element, such as B, As, Cs, I [see *Snyder et al.*, 2005], or N [*Sadofski and Bebout*, 2003], and more like Th and the immobile rare earth elements (REE) and high field strength elements (HFSE).

[22] The U and Th data are consistent with models that presume retention of uranium on the slab to arc depths and beyond (K. Kelley et al., Subduction cycling of U, Th, and Pb, submitted to *Earth and Planetary Science Letters*, 2004). A new geochemical model for arcs, including substantial releases of relatively immobile species such as Be behind the arc front, has been propounded by *Morris et al.* [2002] [see also *Morris and Ryan*, 2003], but further field and geochemical study of cross-arc variations and back-arc regions, especially in the Marianas, are required to confirm these contentions. As the abundances for arsenic and antimony (and to much lesser extend lead) in our forearc serpentinite samples are higher than that of the

Table 2a. (Representative Sample). ICP-MS Trace Element Data for Serpentinized Peridotites From Conical Seamount, Site 779A[a] [The full Table 2a is available in the HTML version of this article at http://www.g-cube.org]

	Core and Section											
	3R-CC	4R-01	5R-02	6R-01	8R-01	8R-01	9R-01	9R-02	10R-01	10R-01	10R-02	11R-01
Interval and piece number	(15–16) # 2	(27–29)	(62–64)	(20–22) # 2	(49–55)	(90–92)	(90–95)	(52–54) # 4B	(17–20)	(106–107)	(33–34) # 1	(16–18) # 3
Depth, mbsf	10.76	20.4	30.82	39.3	59.05	59.43	70.45	70.09	77.91	78.8	79.26	87.46
TiO_2, wt %	0.005	0.010	0.010	0.007	0.011	0.010	0.005	0.003	0.014		0.009	0.001
Al_2O_3	0.36	0.30	0.24	0.48	0.64	0.35	0.32	0.38	0.58		0.32	0.29
Fe_2O_3T	7.08	9.46	8.78	7.66	8.67	8.42	7.51	8.69	9.13		8.68	6.69
MnO	0.10	0.17	0.12	0.10	0.12	0.12	0.10	0.14	0.12		0.16	0.10
MgO	42.99	48.46	47.74	42.29	45.29	46.29	45.04	46.42	47.03		45.15	41.72
CaO	0.21	0.12	0.10	0.45	0.66	0.20	0.48	0.27	0.60		0.10	0.55
Na_2O	0.07	0.06	0.06	0.03	0.07	0.05	0.08	0.01	0.05	0.15	0.15	0.09
K_2O ppm	161	28	61	90	115	49	40	31	108		785	82
L.O.I., %	13.80	17.19	16.62	14.10	11.38	9.56	12.10		6.48	19.24	16.88	17.50
Sc, ppm	6.3			6.1			5.1	4.6			4.3	6.9
V								51.8			24.1	
Cr								1612.3			5049.7	
Ni	2314.3			2289.0			2489.9	493.9			2268.5	2206.4
Sr	1.6	6.9	6.9	7.5	13.1	3.3	7.2	11.7	4.3	9.4	17.3	20.6
Ba	0.7	3.1	1.6	1.0	6.2	1.7	0.8		2.3	0.9		1.8
Rb (USF ICP-MS)			0.196	0.430							0.390	
Cs (USF ICP-MS)			0.094	0.255							0.088	
Pb (USF ICP-MS)			0.105	0.099								
Cu								3.03			6.61	
Zn								76.25			92.82	
B	32.7	57.5	43.3	27.5	14.5	20.4	17.7		17.2	15.9		30.8
Li	10.5	1.4	5.8	9.6	10.3	3.3	2.3		1.4	1.3		3.5

	Core and Section											
	15R-02	15R-02	16R-01	16R-02	17R-01	17R-02	17R-03	17R-03	18R-02	18R-02	19R-02	20R-01
Interval and piece number	(5–6) #1	(22–23) #3	(19–21)	(119–120) #11	(112–114) #14	(14–17)	(76–77) # 8B	(123–125) # 13	(87–89)	(113–114) # 2	(94–95) # 13B	(17–18) # 2B
Depth, mbsf	127.45	127.62	135.73	138.19	146.32	146.87	148.88	149.35	157.28	157.53	161.85	169.27
TiO_2, wt %	0.004	0.001	0.013	0.005	0.008	0.010	0.010	0.003		0.001	0.006	0.001
Al_2O_3	0.61	0.21	0.70	0.84	0.37	0.43	0.30	0.39		0.25	0.23	0.24
Fe_2O_3T	8.87	5.87	8.62	8.87	8.71	8.18	9.14	7.70		8.23	8.83	6.99
MnO	0.16	0.11	0.12	0.13	0.14	0.12	0.15	0.10	0.07	0.12	0.16	0.10
MgO	45.69	43.92	46.44	45.59	46.36	46.68	45.94	44.22		43.20	46.86	
CaO	0.54	0.28	0.61	0.84	0.31	0.41	0.35	0.51		0.16	0.45	0.31

[a] All elements in ppm, except for TiO_2, which is in weight percent. See text for analytical precision.

10.1029/2004GC000777

Table 2b. ICP-MS Trace Element Data for Serpentinized Peridotites From Conical Seamount Site 779A[a]

	Core and Section												
	03R-CC	06R-01	9R-02	10R-02	012R-01	013R-02	14R-01	020R-01	022R-01	026R-02	30R-01	34R-01	35R-01
Interval and piece number	(15–16) # 2	(20–22) # 2	(52–54) # 4B	(33–34) # 1	(16–18) # 3	(53–54) # 1	(82–85) # 5A	(17–18) # 2B	(60–61) # 11	(18–25) # 2C	(82–84) # 1	(62–64) # 5	(8–10) # 1
Depth, mbsf	10.76	39.3	70.09	79.26	97.02	108.63	117.02	169.27	170.71	208.25	245.82	284.32	293.38
Li	9.4	4.0	1.8	3.2	2.9	1.9	6.7	11.2	9.0	1.8	0.6	1.7	2.5
Sc	6.4	6.6	5.3	4.6	4.3	8.2	7.4	6.4	5.5	10.6	4.1	6.3	4.9
TiO_2, wt%				0.003	0.004			0.002	0.004	0.008		0.009	
Cr				757.0	1557.6			2097.6	2449.2	4278.7		2607.9	
Co				119.6	103.2			107.6	105.4	106.9		115.8	
Ni				2364.8	2205.3			2258.8	2252.2	1931.8		2318.2	
Cu	2.2	1.7	2.3	1.6	1.6	6.6	3.7	1.4	1.5	3.6	1.2	4.2	3.9
Zn				12.1	39.1			35.4	55.6	12.8		21.1	
Ga	0.3	0.5	0.2	0.2	0.1	0.5	0.4	0.2	0.2	0.6	0.2	0.3	0.1
As	0.6	0.6	0.6	1.5	0.1	0.5	0.5	0.1	0.2	0.9	0.2	1.2	2.5
Rb	1.044	0.450	0.121	0.261	0.094	0.268	0.904	1.066	0.814	0.448	0.101	0.258	0.112
Sr	1.903	8.217	7.576	16.909	12.297	0.787	1.901	4.872	6.619	6.968	4.136	22.882	13.237
Y	0.030	0.079	0.057	0.018	0.037	0.086	0.050	0.009	0.044	0.086	0.023	0.044	0.014
Zr	0.119	0.104	0.190	0.129	0.167	0.089	0.437	0.462	0.175	0.085	0.106	0.075	0.114
Nb	0.021	0.164	0.277	0.002	0.168	0.025	0.004	0.118	0.194	0.001	0.094	0.001	0.013
Cs	0.29	0.22	0.06	0.06	0.02	0.06	0.15	0.45	0.31	0.14		0.05	0.09
Ba	2.00	2.18	0.79	0.58	0.47	0.67	2.47	1.82	1.46	6.60	0.29	1.16	0.88
La	0.0051	0.0026	0.0038	0.0086	0.0086	0.0022	0.0126	0.0077	0.0124	0.0112	0.0056	0.0049	0.0035
Ce	0.0153	0.0108	0.0140	0.0148	0.0426	0.0096	0.0247	0.0457	0.0507	0.0225	0.0174	0.0103	0.0115
Pr	0.0012	0.0007	0.0010	0.0016	0.0022	0.0007	0.0026	0.0024	0.0037	0.0020	0.0016	0.0011	0.0009
Nd	0.0035	0.0026	0.0024	0.0055	0.0093	0.0022	0.0088	0.0081	0.0146	0.0070	0.0051	0.0045	0.0029
Sm	0.0004	0.0000	0.0005	0.0009	0.0012	0.0002	0.0017	0.0003	0.0017	0.0014	0.0008	0.0009	0.0004
Eu	0.0015	0.0012	0.0005	0.0006	0.0008	*BDL*	0.0011	0.0011	0.0015	0.0040	0.0007	0.0015	0.0005
Gd	0.0008	0.0014	0.0018	0.0014	0.0022	0.0013	0.0020	0.0005	0.0041	0.0019	0.0008	0.0014	0.0008
Tb	0.0002	0.0004	0.0004	0.0003	0.0005	0.0005	0.0005	0.0001	0.0008	0.0005	0.0001	0.0003	0.0001
Dy	0.0033	0.0066	0.0056	0.0027	0.0032	0.0072	0.0049	0.0009	0.0058	0.0065	0.0022	0.0042	0.0011
Ho	0.0010	0.0027	0.0019	0.0005	0.0010	0.0028	0.0015	0.0003	0.0013	0.0029	0.0008	0.0014	0.0005
Er	0.0040	0.0133	0.0081	0.0020	0.0041	0.0143	0.0068	0.0014	0.0058	0.0135	0.0033	0.0057	0.0021
Yb	0.0091	0.0248	0.0163	0.0046	0.0087	0.0310	0.0133	0.0045	0.0093	0.0299	0.0086	0.0122	0.0060
Lu	0.0022	0.0054	0.0028	0.0012	0.0020	0.0065	0.0029	0.0013	0.0022	0.0063	0.0016	0.0026	0.0014
Hf	0.003	0.003	0.005	0.004	0.005	0.003	0.009	0.009	0.006	0.002	0.003	0.002	0.004
Pb	0.06	0.04	0.05	0.02	0.07	0.04	0.04	0.03	0.03	0.02	0.03		0.07
Th	0.0005	0.0005	0.0007	0.0033	0.0009	0.0004	0.0024	0.0004	0.0013	0.0039	0.0006	0.0015	0.0005
U	0.0006	0.0004	0.0007	0.0013	0.0015	0.0002	0.0010	0.0005	0.0005	0.0023	0.0013	0.0026	0.0009
Sb	0.008	0.003	0.005	0.029	0.003	0.006	0.011	0.002	0.001	0.095	0.001	0.258	0.045

[a] All elements in ppm, except for TiO_2, which is in weight percent. See text for analytical precision. BDL = below detection limit.

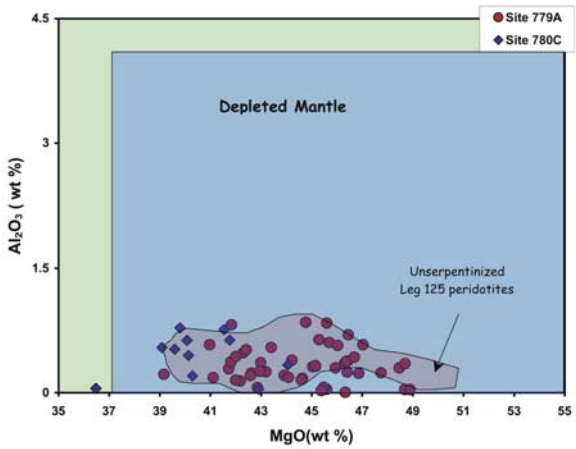

Figure 8. Plot of Al_2O_3 with MgO. Circles are Site 779A; diamonds are Site 780C. Also shown as a dark field is the range of depleted mantle values for these elements [after *Sun and McDonough*, 1989; *Salters and Stracke*, 2004].

depleted mantle, we infer that sulfide mineral(s) are unstable in this setting, permitting the mobility of these species in hydrous fluids. The depleted $\delta^{34}S$ signature of the Leg 125 fluids described in *Mottl and Alt* [1992] support this contention.

5.2.4. Rare Earth Element (REE) Systematics

[23] All of the measured REE abundances are very low and consistent with those observed in studies of less serpentinized Leg 125 peridotites [*Parkinson et al.*, 1992) (Tables 1b and 2b). Conical Seamount samples display "U" shaped patterns with elevated light rare earth elements (LREE) ($[La/Sm]_N = 3.1–37.6$), positive Eu anomalies, and variable heavy rare earth elements (HREE). U-shaped REE patterns are common features in harzburgites from the lower parts of ophiolite successions, such as Vourinos, Twin Sisters, Oman, the Urals, and Trinity [*Sharma and Wasserburg*, 1996; *Gruau et al.*,

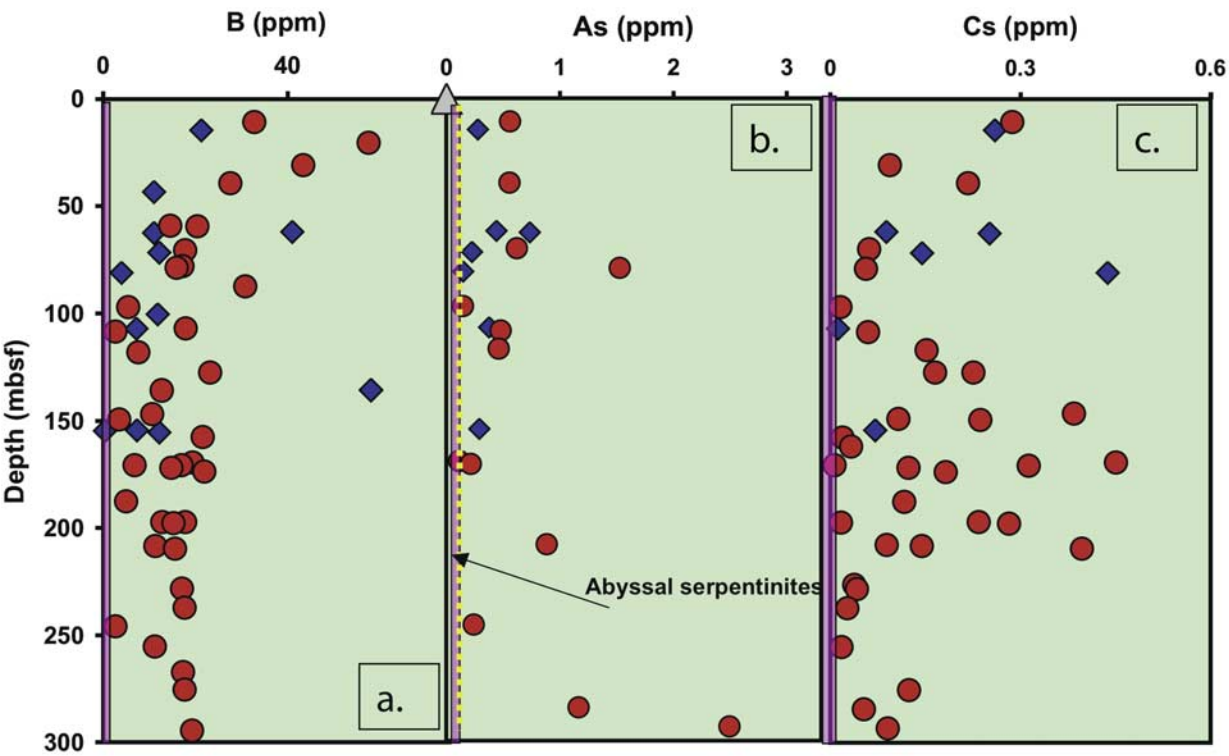

Figure 9. Elemental variations with increasing core depth: (a) B; (b) As (abyssal serpentinite data are unpublished As data of I. P. Savov et al. (2003)); (c) Cs; (d) Sb; (e) Li; (f) Rb; (g) Sr; (h) Ba; (i) Pb; (j) Th; (k) U. mbsf, meters below seafloor. Squares in Figure 9e are serpentinized peridotites from Site 778A, and the large triangle represents seawater. All other symbols are the same as in Figure 8. The transparent rectangular area represents the range of depleted mantle values for the elements of interest. Depleted mantle values are from *Sun and McDonough* [1989] and *Salters and Stracke* [2004]; seawater values are from the GERM reservoir Web site (http://earthref.org/GERM/index.html).

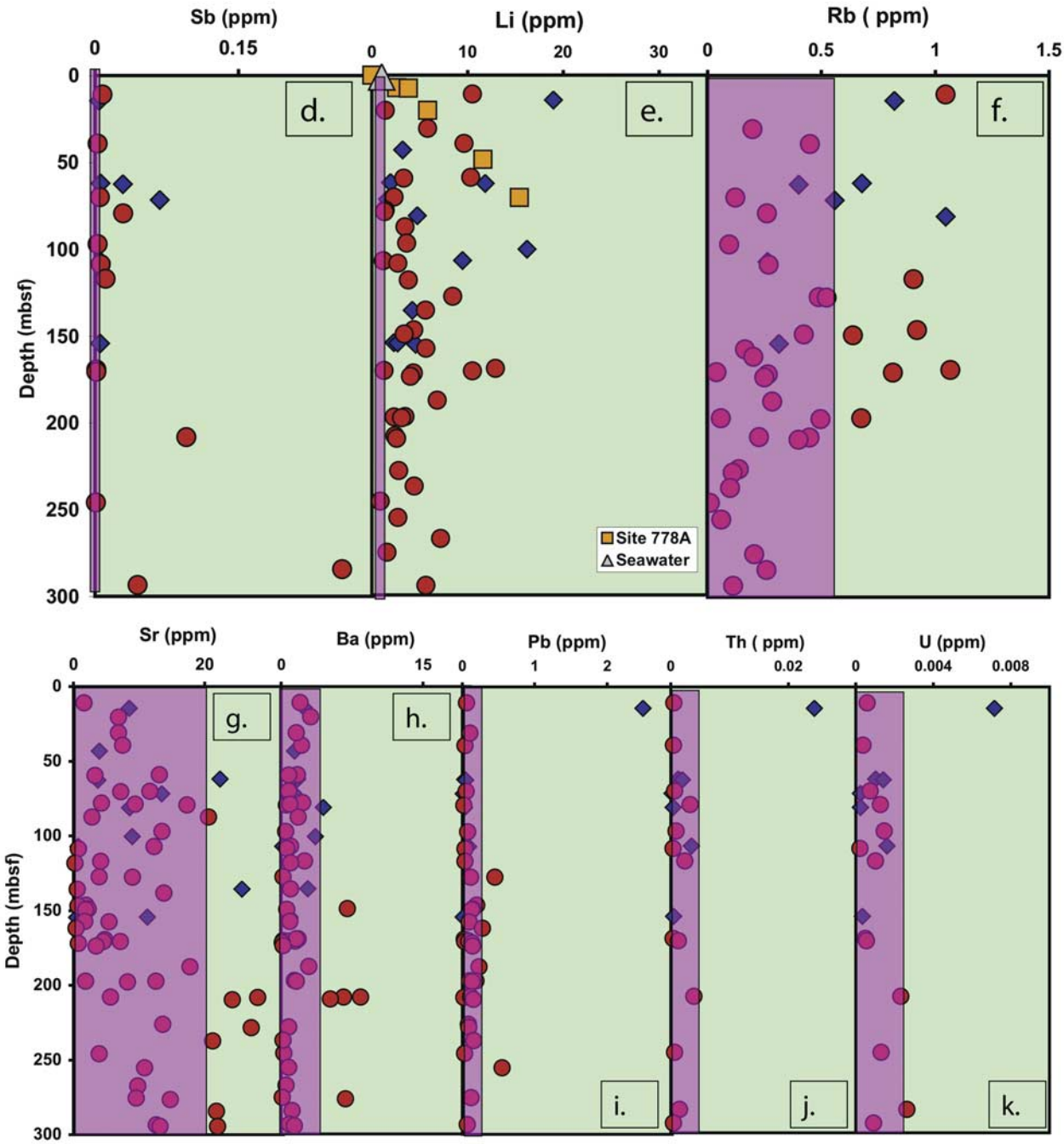

Figure 9. (continued)

1998]. *Gruau et al.* [1998] argued that low-temperature hydrothermal alteration by fluids derived from the continental crust was responsible for the U-shaped REE patterns and positive Eu anomalies in serpentinized harzburgites. However, large volumes of continental materials are not present in the arc-trench gap of the IBM subduction system [see *Fryer et al.*, 1992; *DeBari et al.*, 1999; *Plank et al.*, 2000]. LREE-enriched fluids (with anomalously elevated Eu) have been reported from active hydrothermal fields along the East Pacific Rise [*Langmuir et al.*, 1997; *Douville et al.*, 1999]. *German et al.* [1999] notes that hydrothermal sediments that interact with LREE-depleted Eu-enriched fluids preserve the fluid-like LREE-depleted patterns. The absence of REE correlations with LOI (Figure 6), and the similarity of the REE patterns in all of the studied samples (Figure 10) suggests that the Leg 125 serpentinites preserve the REE signatures of their protoliths. The REE sig-

natures of these serpentinized peridotites are similar to those reported by *Parkinson et al.* [1992], confirming that the REE patterns of Conical Seamount serpentinites are caused by the combination of high degree melting, and the subsequent fluxing of the subarc mantle with LREE-enriched fluids or melts. In intraoceanic settings, melts or fluids with such characteristics are developed only beneath arcs. The positive Eu anomalies probably relate to the reducing environment that develops after extensive serpentinization [*Mottl*, 1992] and can stabilize Eu^{2+}. According to *Noll et al.* [1996], similar processes are commonly observed in hydrothermal ore and banded iron formations worldwide. The positive slopes of the HREE ([range of $Gd/Yb]_N$ = 0.03–1.3) indicate mantle protoliths that were very depleted. Except for the Eu anomalies, the REE patterns of our serpentinites resemble those of western Pacific boninites [*Parkinson et al.*, 1992, *Pearce et al.*, 1999; *Deschamps and Lallemand*, 2003]. The less hydrated serpentinites of the Leg 125 suite have been modeled as boninite source rocks [*Parkinson et al.*, 1992]. Our results are consistent with evidence that point to a complex array of processes governing boninite production [*Crawford et al.*, 1989], including the melting of variably hydrated (serpentinized) peridotites as a means of boninite genesis.

5.2.5. High Field Strength Elements Systematics (Ti, Zr, Hf, Nb)

[24] Our Conical Seamount samples have low zirconium, hafnium, and titanium abundances compared to the depleted mantle values of *Salters and Stracke* [2004], and Nb abundances that range both higher and lower than depleted mantle (Figure 11). LOI values and HFSE/Yb ratios do not correlate in our data set (Figure 6). *Woodhead et al.* [1993] note that high degree fluxed melting of the mantle wedge is necessary to explain the HFSE systematics in primitive arc lavas (i.e., the higher Ti/Zr and Ti/Eu ratios of primitive arc lavas relative to MORBs). *Brenan et al.* [1994] and *Tatsumi and Nakamura* [1986] have shown that the HFSE remain immobile under low temperature hydrous conditions, with abundance patterns controlled entirely by source abundances and extent of melting. As with the REE, HFSE systematics of our Conical Seamount samples in general support a model of high degrees of melt extraction from mantle protoliths, as previously discussed by *Parkinson et al.* [1992] and *Parkinson and Pearce* [1998]. The variation in our Nb data appears to be real, and is difficult to reconcile with general models of melt extraction. One possible explanation is localization of Nb in oxide phases, which may be heterogeneously distributed on the scale of sampling.

5.3. Strontium Isotopes

[25] The Mariana forearc serpentinized clasts have $^{87}Sr/^{86}Sr$ ratios that show no relationship to LOI, and are much lower than seawater $^{87}Sr/^{86}Sr$ (Table 3; Figure 4). The serpentinite sample with the highest $^{87}Sr/^{86}Sr$ comes from near the top of the section (~0.7054), while deeper samples decline to uniform and less radiogenic ratios (~0.7049) (Figures 4a and 4b). Our Sr isotopic data complement the results of *Haggerty and Chaudhuri* [1992], which show that interstitial waters from the unconsolidated serpentinite muds have $^{87}Sr/^{86}Sr$ between 0.7091 and 0.70525. Both data sets indicate that the high $^{87}Sr/^{86}Sr$ in deep pore fluids and serpentinized peridotites record interaction with a non-seawater high $^{87}Sr/^{86}Sr$ source.

5.4. Constraining Seawater Interactions

[26] While seawater contributions for many of the species examined here are likely to be negligible, elements such as Na, Ca, Sr, K, and B, and the isotopic signatures of Li, B, Sr, O and H, may be drastically impacted by seawater exchange. Multiple geochemical indicators argue against deep seawater penetration at Conical Seamount. Recovered porefluids (below 15 m at Hole 780, and below 80 m at Hole 779) have very high pH (always >10, reaching 12.6 in Hole 780), high alkalinity (40 to 120 mmol/kg), Na/Cl ratios between 1.15 and 1.2, and high B and K contents (>3000 μmol/mg B and >18 mmol/kg K; by comparison seawater contains 420 μmol/kg B and 10.2 mmol/kg K [*Mottl*, 1992]). These fluids are also anomalously low in Ca, Mg, Li, Cl, Br Mn, Ba, Si and $\delta^{34}S$ [*Mottl*, 1992], supporting an origin via slab-dehydration reactions at depth.

[27] Near the ocean floor, the upward-migrating deep fluids meet seawater (Ca-rich and with much lower pH), triggering the precipitation of needle-like aragonite crystals, often >1 cm in size, within the serpentinite muds. The presence/absence and relative abundance of aragonite crystals can be used to estimate the depth of seawater penetration into the seamounts. At core depths of 0 to 5 mbsf, $CaCO_3$ contents in the muds may be as high as 36 wt% (for site 779A) and 20 wt% (for site 780C), dropping to values <1% below ~10 mbsf [*Mottl*, 1992].

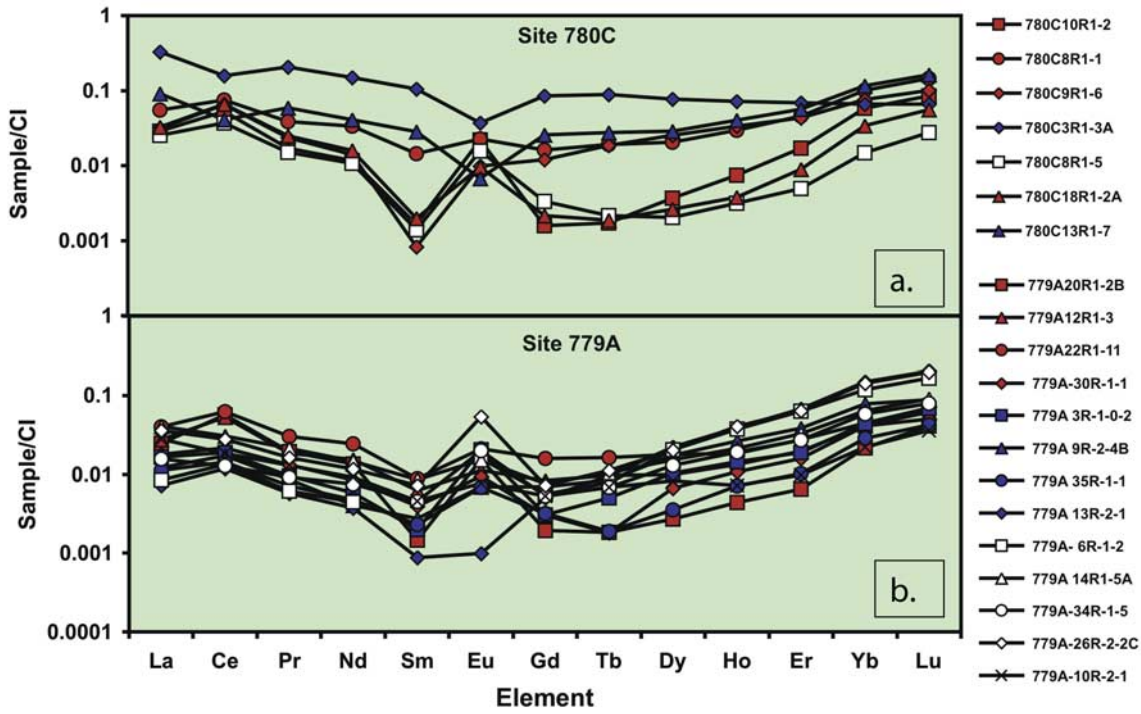

Figure 10. Coryell-Masuda diagram for selected samples from Conical Seamount, ODP Leg 125, Sites (a) 780C and (b) 779A. Note the very low abundances, the overall U-shaped patterns, and the positive Eu anomalies. Chondrite meteorite (CI) values are from *Nakamura* [1974].

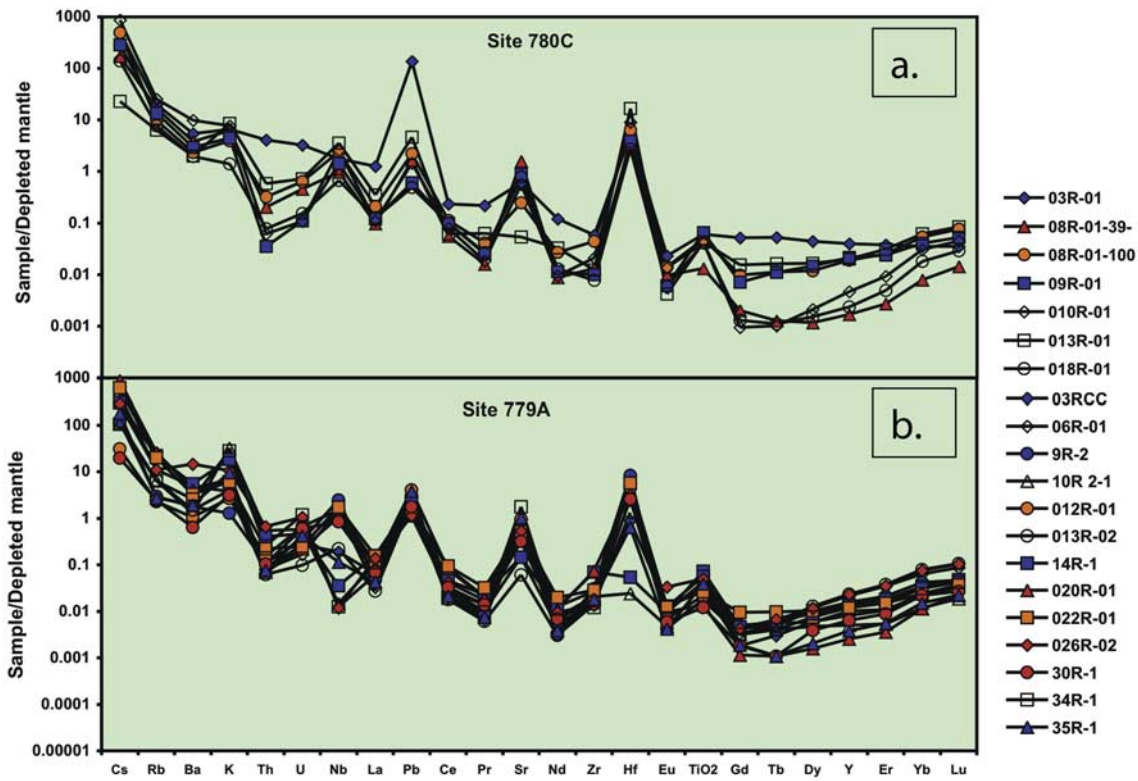

Figure 11. Depleted mantle-normalized multielement plot for selected samples from Conical Seamount, ODP Leg 195, Sites (a) 780C and (b) 770A. Note the large LILE enrichments and the depletions of the HFSE and REE. Depleted mantle values are from *Sun and McDonough* [1989] and *Salters and Stracke* [2004].

Table 3. The $^{87}Sr/^{86}Sr$ of Serpentinized Peridotites From Conical Seamount

Sample	Sr, ppm	L.O.I., %	$^{87}Sr/^{86}Sr$	2s	Depth, mbsf
11 R1 (16–18) # 3	20.6	17.5	0.705342	0.000008	87.46
12 R1 (16–18) # 3	13.5	18.4	0.705422	0.000007	107.1
24 R1 (34–36) # 6	17.8	18.5	0.704939	0.000008	187.54
26 R3 (103–104) # 3B	24.2	15.2	0.704891	0.000007	209.54
29 R2 (131–133) # 1	21.2	19.1	0.704739	0.000006	237.21

[28] Low δD and high $\delta^{18}O$ values in Conical Seamount porefluids and muds also suggest that the porefluids are derived from mineral dehydration reactions at depth [*Benton*, 1997]. B abundance and B isotopic ratios in the serpentinites are sensitive to the complex changes in pH and pore water chemistry associated with seawater infiltration [*Benton et al.*, 2001] and suggest greater depths of seawater influence than other parameters: ~15 m at Hole 780, and possibly ~100 m at Hole 779. Similarly, the strong difference in $^{87}Sr/^{86}Sr$ between seawater (present-day ~0.7092) and the IBM sub-arc mantle ($^{87}Sr/^{86}Sr$ ~ 0.7024–0.7042 [*Hickey-Vargas*, 1998; *Ishikawa and Tera*, 1999; *Hochstaedter et al.*, 2001)] can also be used to identify downcore seawater-peridotite interactions (Figure 4).

6. Implications

6.1. Can Serpentinized Peridotites in the Forearc Play a Role in Generating Island Arc Lava Geochemical Signatures?

[29] Mantle peridotites are the dominant lithology contributing to the geochemical signature of arc source regions. However, since the upper mantle has a relatively simple mineralogy (OL + OPX ± CPX ± Sp), it is poor in chemical species other than Mg, Si, Fe, Mn, Cr, and Ni. Thus, in most arc petrogenetic models [*Plank and Langmuir*, 1998; *Ishikawa and Tera*, 1999; *Hochstaedter et al.*, 2001], the sources for arc lava elemental enrichments are characterized on the basis of the geochemical inventory of the subducting slab. During subduction, increasing pressures, temperatures and tectonic stresses in forearc regions trigger mineral transformations on the slab that result in large scale fluid expulsion [*Tatsumi and Eggins*, 1997; *Schimdt and Poli*, 1998, 2003; *Hyndman and Peacock*, 2003].

[30] To place a broad constraint on the magnitude of the forearc reservoir (and thereby on likely forearc elemental releases from the slab), we have estimated the mass transfer of elements which might occur if 100% of the slab-derived fluids released beneath the forearc were incorporated into forearc mantle serpentinites. According to *Schmidt and Poli* [1998], ~5.5 wt% H_2O leaves subducting Pacific slabs under forearc (blueschist) conditions, which represents slab depths between 20 and 60 km. The mass of water in subducting basalts is $\sim 0.55 \times 10^9$ g/m^2 of slab surface; in gabbros: $\sim 0.15 \times 10^9$ g/m^2, and in subducted trench sediments it is 0.015×10^9 g/m^2 [see also *Schmidt and Poli*, 2003]. The total water available in the subducting column is $\sim 7.15 \times 10^8$ g/m^2 (or $\sim 1.3 \times 10^8$ g/m^2/percent water loss during blueschist facies metamorphism). The above constraints give us a total water loss from the highly altered subducted crust under the Mariana forearc of $\sim 5.85 \times 10^8$ g/m^2. Calculating the dehydration-related water release occurring under the entire volume of the forearc and over ~1000 km subduction zone length yields $\sim 5 \times 10^{16}$ kg of H_2O. This mass is only ~0.0114 of the mass of the forearc mantle, using peridotite densities of 3.4 g/cm^3. The mass of mantle peridotite in the Mariana forearc wedge is $\sim 4.4 \times 10^{18}$ kg, and the mass of serpentinite formed in the forearc via incorporation of released slab fluids (using serpentinite density of 2.5 g/cm^3) is in the order of $\sim 6 \times 10^{17}$ kg (assuming water is incorporated into peridotite up to ~12 wt% to produce serpentine minerals [*O'Hanley*, 1996]). Thus ~13% of the Mariana forearc mantle would be serpentinized by slab-released fluids under Mariana forearc between 20 and 60 km depths.

[31] To estimate likely percentages of element transfer from slab to forearc mantle, we calculate and compare the mass of a given element in the Mariana slab inventory and in the serpentine produced by slab dehydration. Abundances of elements in the sedimentary and basaltic portions of the slab are based on ODP Leg 185 results [*Plank et al.*, 2000; *Kelley et al.*, 2003; *Staudigel*, 2003; *Schmidt and Poli*, 2003]; the concentrations in serpentinites are based on the data shown in Tables 1a, 1b, 2a, 2b, and 4b; and depleted mantle values follow *Salters and Stracke* [2004]. The total mass of any species added to the forearc (mass of

Table 4a. Parameters Used in the Mass Balance Calculations Discussed in the Text[a]

Parameter	Value
Pacific slab angle	20
Convergence rate, mm/yr	40
Length of the subducted Mariana slab, km	1000
Forearc hydrous phases, %	12
H_2O release in blueschist facies metamorphism, %	5
Length of slab needed for 100% serpentinization, km	85 400
Myr of active subduction for 100% serpentinization	21.5
Slab area under Mariana Forearc at 10–40 km depth, m^2	8.5×10^{10}
Volume of the Mariana Forearc, m^3	1.28×10^{15}
Mass of peridotite mantle, kg	4.36×10^{18}
Mass of H_2O in forearc mantle, kg	5×10^{16}
Mass of the serpentinized mantle, kg	6.07×10^{17}
Mass of the subducted slab [AOC + sediment], kg	1.4×10^{22}

[a] Subduction rates and Pacific slab dip angle are from *Stern et al.* [2004]; depth to the slab is from *Fryer et al.* [1990, 1992]; dehydration rates, mantle wedge mineralogy, and H_2O content are from *Schmidt and Poli* [1998, 2003] and *Hyndman and Peacock* [2003]. We used the following densities: dry peridotite = 3.4 g/cm^3; AOC = 3 g/cm^3; Mariana Trench sediments = 1.86 g/cm^3 [*Plank and Langmuir*, 1998].

element in serpentinite minus mass of element in depleted mantle) is divided by the inventories in the slab (total mass of element in sediments plus total mass of element in basaltic crust). Compared to elemental inventories on the downgoing Pacific slabs, our estimates for the forearc serpentinite "reservoir" suggest large elemental releases in forearcs (Tables 4a and 4b).

[32] If Pacific slabs sustained their current subduction dip and convergence rates for the entire ~50 Ma history of active subduction in the Marianas (20° and 40 mm/yr, respectively) [*Stern et al.*, 2004], the fluid released in the forearc regions between 10 and 40 km depths would be capable of transforming all of the available mass of mantle wedge peridotites into serpentine two times. Our observations of core materials from Conical Seamount (ODP Leg 125) and of samples recovered by dredging or push coring at other serpentinite mud volcanoes [*Fryer et al.*, 1999], demonstrate that the forearc is not completely serpentinized. Relatively unaltered peridotites are found in many forearc sites [*Parkinson and Pearce*, 1992, 1998; *Pearce et al.*, 2000; *Savov*, 2004], suggesting that serpentinization is not pervasive, confirming the observation of *Hyndman and Peacock* [2003] that the mantle wedge includes regions that remain largely dry. Moreover, if the entire volume of the shallow forearc peridotites is fully serpentinized, the density difference between harzburgite (~3.4 g/cm^3) and serpentinite (~2.5 g/cm^3) would trigger volume expansion resulting in vertical uplift of the forearc wedge on the order of ~7 km. The shallow Mariana forearc is currently under water depths of ~3 km, and aside from some nearby oceanic plateaus, the seafloor does not indicate such uplift. Although there is evidence for large extents of serpentinization of the IBM forearc [see *Hyndman and Peacock*, 2003, and references therein], it seems necessary that a continuous input of unmodified mantle peridotite must occur into parts of the forearc to accommodate the combination of large fluid expulsions from the subducted slab (~5.8×10^8 g/m^2 of slab) and the presence of unserpentinized peridotites. It is thus probable that highly serpentinized peridotites are down-dragged toward arc source regions (replaced by influx of dry mantle wedge peridotites), as suggested by *Tatsumi* [1986] and more recently by *Straub and Layne* [2002] and *Hattori and Guillot* [2003]. B and B isotope systematics, as well as Cl, F and LILE evidence from melt inclusions in Izu-Bonin arc tephras also support such a model [*Straub and Layne*, 2002, 2003].

6.2. Insights Into Chemical Recycling During Subduction

[33] Low REE abundances, U-shaped rare earth patterns, variable but low HFSE abundances, and low Al_2O_3 contents all indicate that the protoliths of the Mariana forearc serpentinites are highly residual peridotites, reflecting ~20% melt extraction. Large but selective enrichments of lithophile trace elements in the serpentinites reveal a distinctive geochemical signature produced through the shallow extraction of fluids from the subducted Pacific slab. The Mariana forearc serpentinites are thus complementary to the Franciscan subduction complex forearc suites [*Bebout and Barton*, 1993; *Bebout et al.*, 1999; *Sadofsky and Bebout*, 2003; *King et al.*, 2003], and the elemental enrichments reflected in these rocks must be subtracted from

10.1029/2004GC000777

Table 4b. Elemental Concentrations, Mass, and Calculated Slab Depletions in the Forearc[a]

	B	Cs	As	Li	Sb	Ba	Pb	Rb	U	Th
Average Leg 125 serpentinite concentration (this study), ppm	15.4	0.27	0.48	4.63	0.021	2.11	0.038	0.45	0.001	0.0014
Depleted mantle, ppm	0.05	0.0013	0.0074	1.56	0.0026	1.2	0.023	0.088	0.0047	0.0137
Total available from subducted Pacific AOC, kg	6.3×10^{12}	1×10^{11}	4×10^{11}	1.3×10^{12}	8×10^{10}	2.5×10^{13}	4.8×10^{11}	2.4×10^{12}	4.6×10^{10}	2.1×10^{11}
Total available from subducted Mariana Trench sediment value, kg	5.5×10^{12}	4.14×10^{11}	1.3×10^{12}	1.5×10^{13}	3×10^{10}	2×10^{13}	5.3×10^{11}	1.2×10^{13}	3.8×10^{11}	3×10^{11}
Total available on the slabs under Mariana Forearc, kg	1.2×10^{13}	5.2×10^{11}	1.7×10^{12}	1.6×10^{13}	1.1×10^{11}	4.5×10^{13}	1×10^{12}	1.5×10^{13}	4.3×10^{11}	5.1×10^{11}
Mass of element in the Mariana Forearc before serpentinization, kg	2.2×10^{11}	5.7×10^{9}	3.2×10^{10}	6.8×10^{12}	1.1×10^{10}	5.2×10^{12}	1×10^{11}	3.8×10^{11}	2×10^{10}	6×10^{10}
Mass of element added to the Mariana Forearc, kg	9.3×10^{12}	1.6×10^{11}	2.9×10^{11}	2.8×10^{12}	1.27×10^{10}	1.3×10^{12}	2.2×10^{10}	2.7×10^{11}	5.5×10^{8}	8.2×10^{8}
Calculated Mariana Forearc element reservoir mass, kg	9.6×10^{12}	1.7×10^{11}	3.2×10^{11}	9.6×10^{12}	2.4×10^{10}	6.5×10^{12}	1.2×10^{11}	6.6×10^{11}	2.1×10^{10}	6.1×10^{10}
Mariana serpentinized Forearc reservoir conc., ppm	2.2	0.024	0.07	2.2	0.006	1.48	0.03	0.15	0.005	0.0137
Forearc outflux (% depletion of the subducting slab inventory)	79	32	17	18	12	3	2	2	1	0

[a] The lithologies, geochemistry, and densities are as follows: Mariana Trench sediments [*Plank and Langmuir*, 1998]; Pacific altered oceanic crust [AOC]: *Kelley et al.* [2003] and *Staudigel* [2003], depleted mantle: *Sun and McDonough* [1989], *Salters and Stracke* [2004], and the GERM Web site. In the calculations the entire volume of the forearc between 0 and 10 km is not considered because the H_2O budgets there are strongly affected by fluids leaving the sediment column, without mineral dehydration reactions taking place, much like at accretionary prisms [see *You et al.*, 1993, 1995]. Subtracted were also ~10 km of forearc crust assuming possible presence of trapped Philippine Sea Plate oceanic crust [*Stern et al.*, 2004].

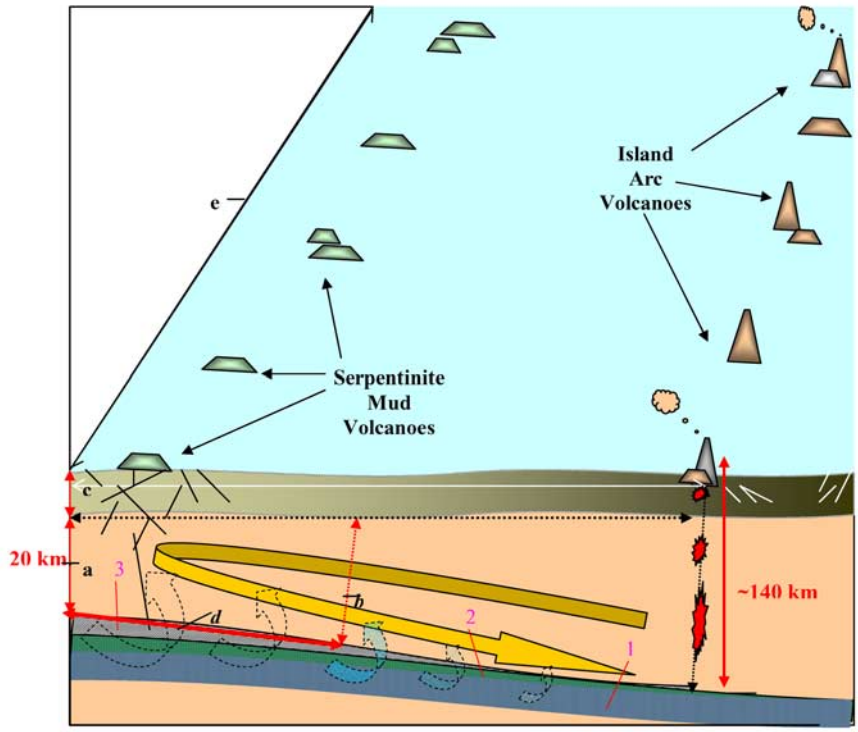

Figure 12. Cartoon illustrating a cross section through the Mariana subarc mantle wedge region discussed in the text [see also *Stern et al.*, 2004]. The main features in our slab inventory depletion calculations are as follows: 3, 2, and 1 are subducted sediments (500 m), altered basaltic crust (3.5 km), and gabbroic crust (3.5 km), respectively. Note the thinning of the sedimentary column with progressive subduction. The forearc mantle wedge dimensions we used are as follows: min. forearc depth (a) = 10 km; max. forearc depth (b) = 40 km; thickness of the forearc crust (c) = 10 km [*Stern et al.*, 2004]; length of the slab currently dehydrating under the Mariana forearc (d) = 85.4 km; section of arc considered for the calculations (e) = 1000 km. The arrow size indicates volume of fluid releases in the subarc region (consistent with the models of *Schmidt and Poli* [1998] and *Hyndman and Peacock* [2003]). Note that the amount of fluid expulsion from the subducting slab is gradually decreasing with increasing depth. We used 20° Pacific slab dip angle for the region between 10 and 40 km (the depth of active mud volcanism and blueschist facies metamorphism).

slab inventories before accurate mass balance calculations for arcs and deep mantle recycling are attempted.

[34] To estimate the cycles for different lithophile elements, we adapt the classic *Plank and Langmuir* [1998] model, i.e., [subduction flux] = [incoming slab flux] + [erosion flux] − [underplating flux] − [accretion flux], substituting forearc output for the accretion flux, as accretion is not believed to occur in the Marianas [*Stern et al.*, 2004, and references therein].

[35] The results of our calculations are outlined in Figure 12 and in Tables 4a and 4b. We presume the "forearc" represents all mantle between 10 and 40 km depth-to-slab, as this encompasses the depth range of the Mariana serpentinite seamounts. What is clear is that the forearc "reservoir" is selective, playing a role in the subduction zone budgets of relatively few elements. However, for these elements (in particular B, As, Cs and Li) the importance of this reservoir is substantial (Tables 4a and 4b). The amount of water released every year from 1 m^2 section of the entire dehydrating portion of Pacific slabs under the Mariana forearc is in the order of $\sim 2.4 \times 10^{10}$ kg/yr. Given that ~12% H_2O can be hosted in serpentine [*O'Hanley*, 1996; *Schmidt and Poli*, 1998], the amount of serpentine that this water can produce from fresh unaltered peridotite mantle is $\sim 2 \times 10^{10}$ kg/yr. The amount of B incorporated annually into the serpentinized peridotites may be $\sim 3 \times 10^6$ kg/yr, and the amount of subducted B at the Mariana Trench is on the order of $\sim 5.5 \times 10^6$ kg/yr (B data for the subducted slab inventory after *Staudigel* [2003, and references therein]). Comparing the subducting slab inputs with the forearc outputs shows that in the case of B, more than half of the entire slab inventory of this element may be released in forearc regions. This inferred B enrichment of the

forearc mantle wedge is consistent with the inferences of cross-arc studies that show little or no B is subducted past arcs [e.g., *Ishikawa and Nakamura*, 1994; *Ryan et al.*, 1996; *Noll et al.*, 1996]. Forearc inventories of As and Sb may be similarly substantial, but our constraints on the slab input of this and other chalcophile species are much poorer.

[36] In contrast to the contentions of *Spandler et al.* [2004] and *Tenthorey and Herman* [2004], our results provide evidence for the substantial removal of slab-derived species into serpentinites in the Mariana forearc (Tables 4a and 4b). We suggest that the forearc plays a very important role in the geochemical cycles of fluid-mobile elements. However, our understanding of the role of forearcs in subduction zone geochemistry is incomplete, because the actual fluid outfluxes associated with serpentinite generation are unknown. Studies of exposed on-land forearc serpentinites (such as within the Franciscan mélange in California [*Bebout et al.*, 1999; *King et al.*, 2003], may help improve our understanding of the three-dimensional structure of the serpentinite seamounts, toward quantifying the extent of mantle-fluid interaction and thereby of shallow FME outfluxes. Given the diverse and at times surprising behaviors of key trace species in forearc settings, documentation of the specific slab sources of these shallow depletions (i.e., sediment- versus altered crust-derived fluids) may require an approach different from that taken in the study of arcs.

Acknowledgments

[37] This research constituted part of Ivan Savov's doctoral dissertation, and was supported by NSF grants EAR 9205804, EAR 9304133, and OCE 9977036 to Ryan and by *JOI/USSAC* Leg 195 postcruise science support grant to Savov and Ryan. The help of Terry Plank, who hosted the first author and allowed open access to her ICP-MS Facility at Boston University, is appreciated. We thank Ilenia Arienzo for her help with the Sr isotope analyses at Osservatorio Vesuviano. Nathan Becker and Patty Fryer are thanked for allowing us to use their maps of the Conical Seamount. The authors appreciate the advice and the stimulating discussions with Patty Fryer, Mike Mottl, Mette Kristensen, Julian Pearce, Sonia Tonarini and Thomas Zack. Serpentinized peridotite samples from ODP Sites 637A, 895D, 897D and 920D were provided by Jeff Alt. Reviews by M. Scambelluri, S. Sadofski, R. King, and G. Bebout significantly improved the quality of the paper. This research used samples and/or data provided by the Ocean Drilling Program. ODP is sponsored by the U.S. National Science Foundation (NSF) and participating countries under the management of Joint Oceanographic Institutions (JOI), Inc.

References

Bailey, E. H., and K. V. Ragnarsdottir (1994), Uranium and thorium solubilities in subduction zone fluids, *Earth Planet. Sci. Lett.*, *124*, 129–191.

Bebout, G. (1995), The impact of subduction-zone metamorphism on mantle-ocean chemical cycling, *Chem. Geol.*, *126*(2), 191–218.

Bebout, G., and M. D. Barton (1993), Metasomatism during subduction: Products and possible paths in the Catalina Schist, California, *Chem. Geol.*, *108*, 61–92.

Bebout, G., J. G. Ryan, W. Leeman, and A. Bebout (1999), Fractionation of trace elements by subduction-zone metamorphism—Effect of convergent-margin thermal evolution, *Earth Planet. Sci. Lett.*, *171*(1), 63–81.

Benton, L. D. (1997), Origin and evolution of serpentine seamounts fluids, Mariana and Izu-Bonin forearcs: Implications for the recycling of subducted material, Ph.D. dissertation, Univ. of Tulsa, Tulsa, Okla.

Benton, L., J. G. Ryan, and F. Tera (2001), Boron isotope systematics of slab fluids as inferred from a serpentine seamount, Mariana forearc, *Earth Planet. Sci. Lett.*, *187*(3–4), 273–282.

Benton, L. D., J. G. Ryan, and I. P. Savov (2004), Lithium abundance and isotope systematics of forearc serpentinites, Conical Seamount, Mariana forearc: Insights into the mechanics of slab-mantle exchange during subduction, *Geochem. Geophys. Geosyst.*, *5*, Q08J12, doi:10.1029/2004GC000708.

Bloomer, S., B. Taylor, C. J. MacLeod, R. J. Stern, P. Fryer, J. W. Hawkins, and L. Johnson (1995), Early arc volcanism and the ophiolite problem: A perspective from ocean drilling in the western Pacific, in *Active Margins and Marginal Basins of the Western Pacific*, *Geophys. Monogr. Ser.*, vol. 88, edited by J. Natland and B. Taylor, pp. 1–30, AGU, Washington, D. C.

Brenan, J. M., H. F. Shaw, D. L. Phinney, and F. J. Ryerson (1994), Rutile-aqueous fluid partitioning of Nb, Ta, Hf, Zr, U and Th: Implications for high field strength element depletions in island-arc basalts, *Earth Planet. Sci. Lett.*, *128*, 327–339.

Chaussidon, M., and B. Marty (1995), Primitive boron isotope composition of the mantle, *Science*, *269*, 383–386.

Crawford, A. J., T. J. Fallon, and D. H. Green (1989), Classification, petrogenesis and tectonic setting of boninites, in *Boninites and Related Rocks*, edited by A. J. Crawford, pp. 2–49, CRC Press, Boca Raton, Fla.

DeBari, S., B. Tylor, K. Spencer, and K. Fujioka (1999), A trapped Philippine Sea plate origin for MORB from the inner slope of the Izu-Bonin trench, *Earth Planet. Sci. Lett.*, *174*, 183–197.

Decitre, S., E. Deloule, L. Reisberg, R. James, P. Agrinier, and C. Mével (2002), Behavior of Li and its isotopes during serpentinization of oceanic peridotites, *Geochem. Geophys. Geosyst.*, *3*(1), 1007, doi:10.1029/2001GC000178.

Deschamps, A., and S. Lallemand (2003), Geodynamic setting of Izu-Bonin-Mariana boninites, in *Intra-Oceanic Subduction Systems: Tectonic and Magmatic Processes*, *Geol. Soc. Spec. Publ.*, *219*, 163–185.

Douville, E., P. Bienvenu, J. L. Charlou, J. P. Donval, Y. Fouquet, P. Appriou, and T. Gamo (1999), Yttrium and rare earth elements in fluids from various deep-sea hydrothermal systems, *Geochim. Cosmochim. Acta*, *63*(5), 627–643.

Elliott, T., T. Plank, A. Zindler, W. M. White, and B. Bourdon (1997), Element transport from subducted slab to juvenile crust at the Mariana Arc, *J. Geophys. Res.*, *102*, 14,991–15,019.

Fryer, P., and M. Mottl (1992), Lithology, mineralogy and origin of serpentine muds recovered from Conical and Torishima forearc seamounts, Results of Leg 125 drilling, *Proc. Ocean Drill. Program Sci. Results*, *125*, 343–362.

Fryer, P., and N. C. Smoot (1985), Processes of seamount subduction in the Mariana and Izu-Bonin trenches, *Mar. Geol.*, *64*, 77–90.

Fryer, P., E. L. Ambos, and D. M. Hussong (1985), Origin and emplacement of Mariana Forearc seamounts, *Geology*, *13*, 774–777.

Fryer, P., et al. (1990), *Proceedings of the Ocean Drilling Program: Initial Reports*, vol. 125, Ocean Drill. Program, College Station, Tex.

Fryer, P., et al. (1992), *Proceedings of the Ocean Drilling Program: Science Results*, vol. 125, Ocean Drill. Program, College Station, Tex.

Fryer, P., C. G. Wheat, and M. Mottl (1999), Mariana blueschist mud volcanism: Implications for conditions within the subduction zone, *Geology*, *27*, 103–106.

German, C. R., J. Hergt, M. R. Palmer, and J. M. Edmond (1999), Geochemistry of a hydrothermal sediment core from the OBS vent-field, 21°N East Pacific Rise, *Chem. Geol.*, *155*(1–2), 65–75.

Gharib, J., P. Fryer, and K. Ross (2002), Lithological and mineralogical analysis of serpentine mud samples from the Mariana Forearc, *Eos Trans. AGU*, *83*(47), Fall Meet. Suppl., Abstract T72A.

Gruau, G., J. B. Griffiths, and C. Lecuyer (1998), The origin of the U-shaped rare earth patterns in ophiolite peridotites: Assessing the role of secondary alteration and melt/rock reaction, *Geochim. Cosmochim. Acta*, *62*, 3545–3560.

Haggerty, J. A., and S. Chaudhuri (1992), Strontium isotopic composition of the interstitial waters from Leg 125: Mariana and Bonin forearcs, *Proc. Ocean Drill. Program Sci. Results*, *125*, 397–400.

Hattori, K., and S. Guillot (2003), Volcanic fronts form as a consequence of serpentinite dehydration in the forearc mantle wedge, *Geology*, *31*(6), 525–528.

Hickey-Vargas, R. (1998), Origin of the Indian Ocean-type isotopic signature in basalts from the West Philippine Sea plate spreading centers: An assessment of local versus large scale processes, *J. Geophys. Res.*, *103*, 20,963–20,979.

Hochstaedter, A., J. Gill, R. Peters, P. Broughton, P. Holden, and B. Taylor (2001), Across-arc geochemical trends in the Izu-Bonin arc: Contributions from the subducting slab, *Geochem. Geophys. Geosyst.*, *2*(7), doi:10.1029/2000GC000105.

Horine, R. L., G. F. Moore, and B. Taylor (1990), Structure of the outer Izu-Bonin forearc from seismic-reflection profiling and gravity modeling, *Proc. Ocean Drill. Program Initial Rep.*, *125*, 81–94.

Hyndman, R. D., and S. M. Peacock (2003), Serpentinization of the forearc mantle, *Earth Planet. Sci. Lett.*, *212*, 417–432.

Ishii, T., P. T. Robinson, H. Maekawa, and R. Fiske (1992), Petrological studies of peridotites from diapiric serpentinite seamounts in the Izu-Ogasawara-Mariana forearc, Leg 125, *Proc. Ocean Drill. Program Sci. Results*, *125*, 445–487.

Ishikawa, T., and E. Nakamura (1994), Origin of the slab component in arc lavas from across-arc variation of B and Pb isotopes, *Nature*, *370*, 205–208.

Ishikawa, T., and F. Tera (1999), Two isotopically distinct fluid components involved in the Mariana arc: Evidence from Nb/B ratios and B, Sr, Nd, and Pb isotope systematics, *Geology*, *27*, 83–86.

Kelley, K. A., T. Plank, J. Ludden, and H. Staudigel (2003), Composition of altered oceanic crust at ODP Sites 801 and 1149, *Geochem. Geophys. Geosyst.*, *4*(6), 8910, doi:10.1029/2002GC000435.

King, R. L., M. Kohn, and J. Eiler (2003), Constraints on the petrologic structure of the subduction zone slab-mantle interface from Franciscan Complex exotic ultramafic blocks, *Geol. Soc. Am. Bull.*, *115*(9), 1097–1109.

Langmuir, C., et al. (1997), Hydrothermal vents near a mantle hot spot: The Lucky Strike vent field at 37°N on the Mid-Atlantic Ridge, *Earth Planet. Sci. Lett.*, *148*, 69–91.

Morris, J. D., and J. G. Ryan (2003), Subduction zone processes and implications for changing composition of the upper and lower mantle, in *The Mantle and Core*, vol. 2, *Treatise on Geochemistry*, edited by H. D. Holland and K. K. Turekian, pp. 451–471, Elsevier, New York.

Morris, J. D., J. Gosse, S. Brachfield, and F. Tera (2002), Cosmogenic Be-10 and the solid Earth: Studies in geomagnetism, subduction zone processes, and active tectonics, in *Beryllium: Mineralogy, Petrology, and Geochemistry*, edited by E. S. Grew, *Rev. Mineral. Geochem.*, *50*, 207–270.

Mottl, M. J. (1992), Pore waters from serpentinite seamounts in the Mariana and Izu-Bonin forearcs, Leg 125: Evidence for volatiles from the subducting slab, *Proc. Ocean Drill. Program Sci. Results*, *125*, 373–387.

Mottl, M. J., and J. C. Alt (1992), Data report: Minor and trace element and sulfur isotopic composition of pore waters from Sites 778 through 786, *Proc. Ocean Drill. Program Sci. Results*, *125*, 683–688.

Nakamura, N. (1974), Determination of REE, Ba, Fe, Mg, Na and K in carbonaceous and ordinary chondrites, *Geochim. Cosmochim. Acta*, *38*, 757–775.

Noll, P. D., H. E. Newsom, W. P. Leeman, and J. G. Ryan (1996), The role of hydrothermal fluids in the production of subduction zone magmas: Evidence from siderophile and chalcophile trace elements and boron, *Geochim. Cosmochim. Acta*, *60*(4), 587–611.

O'Hanley, D. (1996), *Serpentinites: Record of Tectonic and Petrological History*, 271 pp., Oxford Univ. Press, New York.

Parkinson, I. J., and J. A. Pearce (1998), Peridotites from the Izu-Bonin-Mariana Forearc (ODP Leg 125): Evidence for mantle melting and melt-mantle interaction in a supra-subduction zone setting, *J. Petrol.*, *39*(9), 1577–1618.

Parkinson, I. J., J. A. Pearce, M. F. Thirlwall, K. T. M. Johnson, and G. Ingram (1992), Trace element geochemistry of peridotites from the Izu-Bonin-Mariana forearc, Leg 125, *Proc. Ocean Drill. Program Sci. Results*, *125*, 487–507.

Pearce, J. A., P. D. Kempton, G. M. Nowell, and S. R. Noble (1999), Hf-Nd element and isotope perspective on the nature and providence of mantle and subduction components in Western Pacific arc-basin systems, *J. Petrol.*, *40*, 1579–1611.

Pearce, J. A., P. F. Baker, S. J. Edwards, I. J. Parkinson, and P. T. Leat (2000), Geochemistry and tectonic significance of peridotites from the South Sandwich arc-basin system, South Atlantic, *Contrib. Mineral. Petrol.*, *139*, 36–53.

Plank, T., and C. H. Langmuir (1998), The chemical composition of subducted sediment and its consequences for the crust and mantle, *Chem. Geol.*, *145*, 325–394.

Plank, T., et al. (2000), *Proceedings of the Ocean Drillings Program: Initial Reports* [CD-ROM], vol. 185, Ocean Drill. Program, Tex. A&M Univ., College Station, Tex.

Reagan, M. K., J. D. Morris, E. A. Herrstrom, and M. T. Murrell (1994), U-series and Be isotope evidence for an extended his-

tory of subduction modification of the mantle below Nicaragua, *Geochim. Cosmochim. Acta*, *58*, 4199–4212.

Ryan, J. G., and C. H. Langmuir (1987), The systematics of lithium abundances in young volcanic rocks, *Geochim. Cosmochim. Acta*, *51*, 1727–1741.

Ryan, J. G., and C. H. Langmuir (1993), The systematics of boron abundances in young volcanic rocks, *Geochim. Cosmochim. Acta*, *57*, 1489–1498.

Ryan, J. G., J. Morris, G. Bebout, and W. Leeman (1996), Describing chemical fluxes in subduction zones: Insights from the "depth-profiling" studies of arc and forearc rocks, in *Subduction Top to Bottom*, *Geophys. Monogr. Ser.*, vol. 96, edited by G. E. Bebout et al., pp. 263–268, AGU, Washington, D. C.

Saboda, K. L., P. Fryer, and H. Maekawa (1992), Metamorphism of ultramafic clasts from Conical Seamount: Sites 778, 779, and 780, *Proc. Ocean Drill. Program Sci. Results*, *125*, 431–443.

Sadofsky, S. J., and G. E. Bebout (2003), Record of forearc devolatilization in low-T, high-P/T metasedimentary suites: Significance for models of convergent margin chemical cycling, *Geochem. Geophys. Geosyst.*, *4*(4), 9003, doi:10.1029/2002GC000412.

Salters, V. J. M., and A. Stracke (2004), Composition of the depleted mantle, *Geochem. Geophys. Geosyst.*, *5*, Q05B07, doi:10.1029/2003GC000597.

Savov, I. P. (2004), Petrology and geochemistry of subduction-related rocks from the Mariana arc-basin system, Ph.D. dissertation, Univ. of S. Fla., Tampa.

Savov, I. P., J. G. Ryan, I. Haydoutov, and J. Schijf (2001), Late Precambrian Balkan-Carpathian ophiolite—A slice of the Pan-African ocean crust?: Geochemical and tectonic insights from the Tcherni Vrah and Deli Jovan massifs, Bulgaria and Serbia, *J. Volcanol. Geotherm. Res.*, *110*, 299–318.

Savov, I. P., J. G. Ryan, L. H. Chan, M. D'Antonio, M. Mottl, and P. Fryer (2002), Geochemistry of serpentinites from the S. Chamorro Seamount, ODP Leg 195, Site 1200, Mariana Forearc—Implications for recycling at subduction zones, *Geochim. Cosmochim. Acta*, *66*, Abstract 670.

Schmidt, M. W., and S. Poli (1998), Experimentally based water budgets for dehydrating slabs and consequences for arc magma generation, *Earth Planet. Sci. Lett.*, *163*, 361–379.

Schmidt, M. W., and S. Poli (2003), Generation of mobile components during subduction of oceanic crust, in *The Crust*, vol. 3, *Treatise on Geochemistry*, edited by H. D. Holland and K. K. Turekian, pp. 567–593, Elsevier, New York.

Sharma, M., and G. J. Wasserburg (1996), The neodymium isotopic compositions and rare earth patterns in highly depleted ultramafic rocks, *Geochim. Cosmochim. Acta*, *60*, 4537–4550.

Snyder, G. T., I. P. Savov, and Y. Muramatsu (2005), Iodine and boron in Mariana serpentinite mud volcanoes (ODP Legs 125 and 195): Implications for forearc processes and subduction recycling, *Proc. Ocean Drill. Program Sci. Results* [online], *195*. (Available at http://www.odp.tamu.edu/publications/195_SR/102/102.htm)

Spandler, C. J., J. Hermann, R. Arculus, and J. A. Mavrogenes (2004), Geochemical heterogeneity and element mobility in deeply subducted oceanic crust: Insights from high-pressure mafic rocks from New Caledonia, *Chem. Geol.*, *206*, 21–42.

Staudigel, H. (2003), Hydrothermal alteration processes in the oceanic crust, in *The Crust*, vol. 3, *Treatise on Geochemistry*, edited by H. D. Holland and K. K. Turekian, Elsevier, New York, pp. 511–535.

Stern, R., M. Fouch, and S. Klemperer (2004), An overview of the Izu-Bonin-Mariana subduction factory, in *Inside the Subduction Factory*, *Geophys. Monogr. Ser.*, vol. 138, edited by J. Eiler, pp. 175–223, Washington, D. C.

Stolper, E., and S. Newman (1994), The role of water in the petrogenesis of Mariana trough magmas, *Earth Planet. Sci. Lett.*, *121*, 293–326.

Straub, S. M., and G. D. Layne (2002), The systematics of boron isotopes in Izu arc front volcanic rocks, *Earth Planet. Sci. Lett.*, *198*, 25–39.

Straub, S. M., and G. D. Layne (2003), Decoupling of fluids and fluid-mobile elements during shallow subduction: Evidence from halogen-rich andesite melt inclusions from the Izu arc volcanic front, *Geochem. Geophys. Geosyst.*, *4*(7), 9004, doi:10.1029/2002GC000349.

Sun, S. S., and W. F. McDonough (1989), Chemical and isotopic systematics of oceanic basalts: Implications for mantle composition and processes, in *Magmatism in the Ocean Basins*, edited by A. S. Sounders and M. J. Norrey, *Geol. Soc. Spec. Publ.*, *42*, pp. 313–346.

Tatsumi, Y. (1986), Formation of the volcanic front in subduction zones, *Geophys. Res. Lett.*, *13*, 717–720.

Tatsumi, Y., and S. Eggins (1997), *Subduction Zone Magmatism*, 211 pp., Blackwell, Malden, Mass.

Tatsumi, Y., and N. Nakamura (1986), Composition of aqueous fluid from serpentinite in the subducted lithosphere, *Geochem. J.*, *20*, 191–196.

Tenthorey, E., and J. Hermann (2004), Composition of fluids during serpentinite breakdown in subduction zones: Evidence for limited boron mobility, *Geology*, *32*(10), 865–868.

Turner, S., C. Hawkesworth, N. Rogers, J. Bartlett, T. Worthington, J. Hergt, J. A. Pearce, and I. Smith (1997), ^{238}U-^{230}Th disequilibria, magma petrogenesis, and flux rates beneath the depleted Tonga-Kermadec island arc, *Geochim. Cosmochim. Acta*, *61*(22), 4855–4880.

Woodhead, J. D., S. Eggins, and J. A. Gamble (1993), High field strength and transition element systematics in island arc and back-arc basin basalts: Evidence for multi-phase melt extraction and a depleted mantle wedge, *Earth Planet. Sci. Lett.*, *114*, 491–504.

You, C.-F., A. J. Spivack, J. H. Smith, and J. M. Gieskes (1993), Mobilization of boron in convergent margins: Implications for the boron geochemical cycle, *Geology*, *21*, 207–210.

You, C.-F., L. H. Chan, A. J. Spivack, and J. M. Gieskes (1995), Lithium, boron, and their isotopes in sediments and pore waters of Ocean Drilling Program Site 808, Nankai Trough: Implications for fluid expulsion in accretionary prisms, *Geology*, *23*, 37–40.

Zack, T., T. Rivers, and S. F. Foley (2001), Cs-Rb-Ba systematics in phengite and amphibole: An assessment of fluid mobility at 2 GPa in eclogites from Trescolmen, Central Alps, *Contrib. Mineral. Petrol.*, *140*, 651–669.

Zack, T., I. P. Savov, and J. G. Ryan (2004), Storage of light elements in the forearc mantle wedge: SIMS measurements of serpentinites from ODP Leg 195, paper presented at 32nd International Geological Congress, Int. Union of Geol. Sci., Florence, Italy.